Trueman ER, Wong TM (1987) The role of the coelom as a hydrostatic skeleton in lingulid brachiopods. J Zool Lond 213: 221–232
Vovel S (1985) Flow-assisted shell reopening in swimming scallops. Biol Bull 169: 624–630
Vogel S (1987) Flow-assisted mantle cavity refilling in jetting squid. Biol Bull 172: 61–68
Vogel S (1988) How organisms use flow-induced pressures. Am Sci 76: 28–34
Wadepuhl M, Beyn W-J (1989) Computer simulation of the hydrostatic skeleton. The physical equivalent, mathematics and application to worm-like forms. J Theor Biol 136: 379–402
Wainwright SA (1970) Design in hydraulic organisms. Naturwissenschaften 57: 321–326
Wainwright SA (1982) Structural systems: hydrostats and frameworks. In: Taylor CR, Johansen K, Bolis L (eds) A companion to animal physiology. Cambridge Univ Press, Cambridge, pp 325–338
Wainwright SA (1988) Axis and circumference – the cylindrical shape of plants and animals. Harvard Univ Press, Cambridge
Wainwright SA, Biggs WD, Currey JD, Gosline JM (1976) Mechanical design in organisms. Arnold, London
Ward DV (1972) Locomotory function of the squid mantle. J Zool Lond 167: 487–499
Ward DV, Wainwright SA (1972) Locomotory aspects of squid mantle structure. J Zool Lond 167: 437–449
Webber DM, O'Dor RK (1985) Respiration and swimming performance of short-finned squid (*Illex illecebrosus*). NAFO Sci Coun Stud 9: 133–138
Webber DM, O'Dor RK (1986) Monitoring the metabolic rate and activity of free-swimming squid with telemetered jet pressure. J Exp Biol 126: 205–224
Wells MJ (1978) Octopus. Chapman and Hall, London
Wells MJ (1990) Oxygen extraction and jet propulsion in cephalopods. Can J Zool 68: 815–824
Wilkens LA (1981) Neurobiology of the scallop. I. Starfish-mediated escape behaviors. Proc R Soc Lond B 211: 341–372
Wilson DM (1960) Nervous control of movement in cephalopods. J Exp Biol 37: 57–72
Winter MA, Hamilton PV (1985) Factors influencing swimming in bay scallops, *Argopecten irradians* (Lamarck, 1819). J Exp Mar Biol Ecol 88: 227–242
Yonge CM (1936) The evolution of the swimming habit in the Lamellibranchia. Mem Mus Hist Nat Belg (2): 77–99
Yonge CM (1973) Functional morphology with particular reference to hinge and ligament in *Spondylus* and *Plicatula* and a discussion on relations within the superfamily Pectinacea (Mollusca: Bivalvia). Phil Trans R Soc Lond B 267: 171–208
Young JZ (1938) The functioning of the giant nerve fibres of the squid. J Exp Biol 15: 170–185

Chapter 7

Muscle Function in Locomotion

J.L. van Leeuwen

Contents

1 Introduction

Most animal locomotor systems are driven by cross-striated muscles under control of a nervous system. Apart from their mechanical function, muscles may also have important sensory functions through the presence of muscle spindles. Much is known about the physiological and structural properties of muscles, owing to a

Neuroregulation Group, Department of Physiology, University of Leiden, P.O. Box 9604, 2300 RC, Leiden, The Netherlands

Advances in Comparative and Environmental Physiology, Vol. 11

great many studies on isolated muscles or muscle fibres. Only recently, our knowledge of muscle performance in vivo (the main topic of this chapter) has increased considerably.

This chapter starts with a general discussion of muscle properties, with emphasis on mechanical aspects. Special attention will be paid to the dynamics of the muscle–tendon complex. Thereafter, techniques for in vivo monitoring of muscular performance will be reviewed. The major part considers the performance and design of muscles in swimming fish, in flying insects, and in running and jumping mammals. Other aspects of muscle function are discussed in Chap. 5 (mechanical stresses in muscles), Chap. 6 (muscle function in soft bodied animals), and Chap. 8 (muscle energetics). The word contraction is used synonymously with shortening in this chapter, and is quite distinct from the term activation (Sect. 2.2). A list of symbols and abbreviations is given in Appendix A.

2 Muscle Properties

Muscle and muscle fibre structure is discussed in many recent textbooks on physiology, cell biology and histology. Here, only a brief summary is given. The various levels of structural organization of a cross-striated muscle are schematized in Fig. 1. The muscle belly – composed of muscle fibres, connective tissue, blood vessels and nerves – is connected to the skeleton via tendons, with collagen fibres as the dominant component. Muscle fibres are elongated multi-nucleated cells, and contain myo-filaments (arranged in sarcomeres: the contractile units), mitochondria (for energy supply) and endoplasmic (sarcoplasmic) reticulum (with an important function in the activation process). Muscle fibres are connected to their tendon(s) via tendinous sheets. In a musculous attachment, muscle fibres insert via very short collagen fibres to the skeleton. Tendons and tendinous sheets act as force transmitters and elastic energy stores (Sect. 2.7). To investigate the function of muscles in locomotor systems, quantitative models of the mechanical behaviour of sarcomeres, muscle fibres and muscle–tendon complexes are required. In the following, such models will be developed, based on quantified phenomenological descriptions of the fundamental properties of underlying structural and functional levels.

2.1 Sarcomeres

The force and mechanical power production of sarcomeres depends on (1) sarcomere length and geometry, (2) shortening velocity, and (3) the activation of the sarcomere. This section deals with the first two aspects; activation dynamics is discussed in Sect. 2.2.

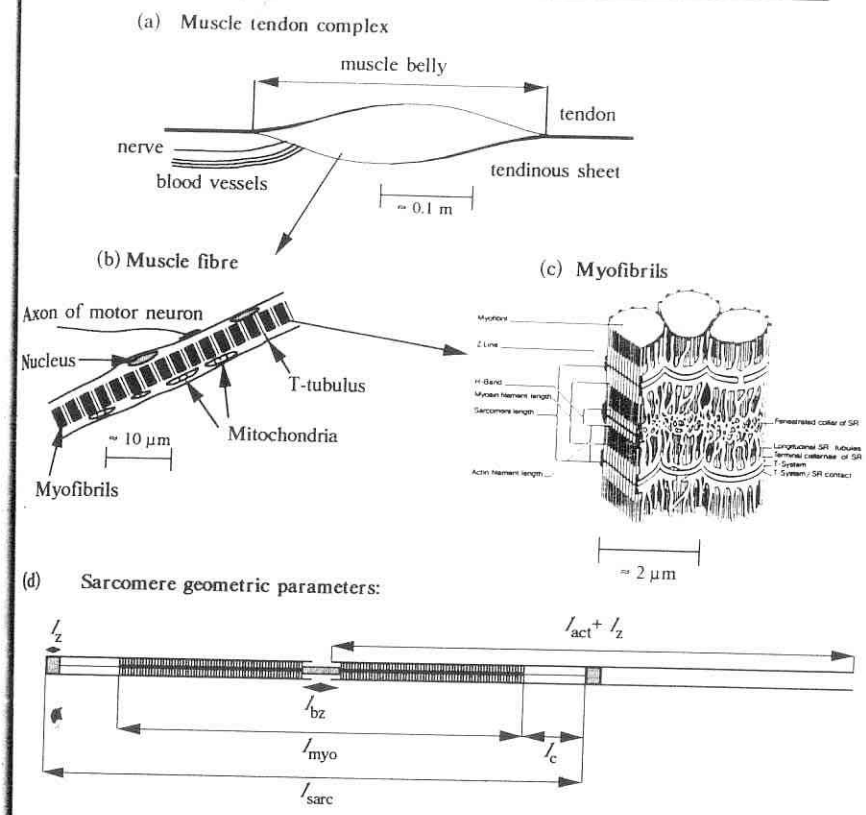

Fig. 1 a–d. Structural organization of cross-striated muscle. **a** Muscle–tendon complex. **b** Muscle fibre with axon terminal of motoneuron, nuclei, mitochondria, T-tubulus and myofibrils. **c** Myofibrils, surrounded by sarcoplasmic reticulum and T-tubuli. (Akster 1981). **d** Geometry of sarcomere model. (Van Leeuwen 1991, but with addition of connecting filament). In one half *Rana* sarcomere subunit about 136 cross-bridges (projecting to six actin filaments) are maximally present. The illustration shows 130 cross-bridges, projecting to only two actin filaments. Symbols are explained in Appendix A. Length scales in **a** to **c** are only approximate

2.1.1 Force Production and Sarcomere Length and Geometry; Filamentary Overlap Function

The main structural elements of the sarcomere (Fig. 1d) are the myosin (thick) filament (with length l_{myo}), the actin (thin) filament (with length l_{act}) and the Z-disc (with thickness l_z). The myosin filament is connected to the Z-disc via the connecting filament (denoted also as titin filament, Wang 1985) of length l_c. From the myosin filament, myosin heads project outwards, except in a central part, the "bare zone",

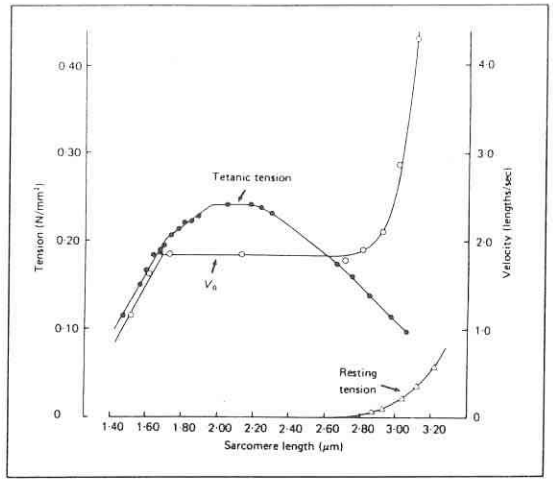

Fig. 2. Tension (*closed symbols*), maximum externally unloaded shortening velocity (*open circles*), and passive forces ($F_{pas\,2}$, *open triangles*) against sarcomere length for a frog muscle fibre. Edman (1979)

of length l_{bz}. In vertebrates, l_{myo} is about 1.6 μm, and seems to vary relatively little (Page and Huxley 1963), in contrast to l_{act} which is highly variable in vertebrates (from about 1.7 to 2.8 μm). The sarcomere length l_{sarc} includes one Z-disc.

Sarcomere length changes are accompanied by sliding movements of the thin filaments past the thick filaments (Sliding filament theory: H.E. Huxley and Hanson 1954; A.F. Huxley and Niedergerke 1954). Cross-bridges are formed by interaction of the myosin heads with neighbouring actin filaments. Experiments (Gordon et al. 1966; Edman 1979) indicate the cross-bridges to be mutually independent generators of force and power (Fig. 2). Thus, under full activation and isometric conditions, the active force production F_{cu0} associated with one half myosin

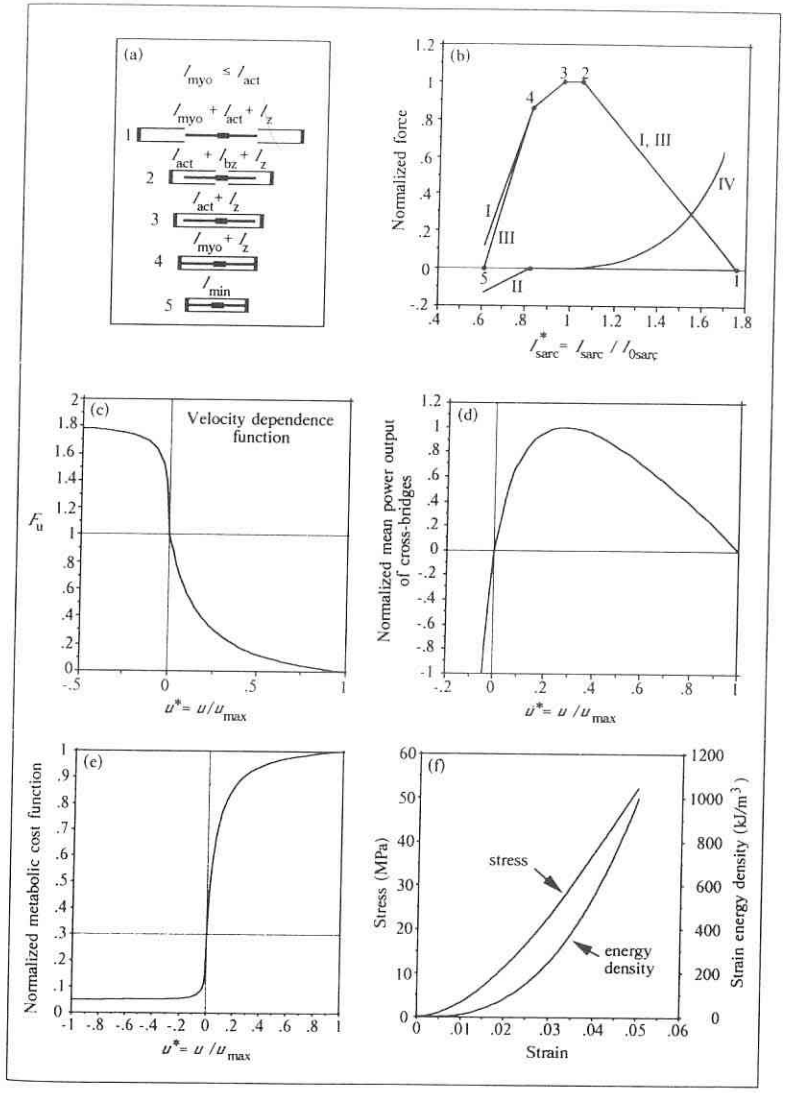

Fig. 3 a–f. Illustration of fundamental mechanical properties of a muscle system. **a** Characteristic lengths (indicated above each pictogram) in a full contraction of a sarcomere are numbered 1 to 5. **b** Force–length relationship of sarcomere with full activation and zero interfilamentary speed. Pictogram numbers of **a** correspond to those given at each characteristic length. Roman numbers denote curves of active force (*I*), $F_{pas\,1}$ (*II*), active force plus $F_{pas\,1}$ (*III*), and $F_{pas\,2}$ (*IV*). **c** Velocity dependence function. **d** Normalized mean cross-bridge power as a function of u^*. **e** Normalized metabolic cost for stress production $P^*_{\sigma}(u^*)$. The left part is an estimate based on a discussion by Woledge et al. (1985). The right part is based on observations by Heglund and Cavagna (1987). **f** Stress–strain relationship of tendinous tissue, based on observations by Ker (1981) and Bennett et al. (1986). A plot is also shown of the strain energy density function, which shows the elastic energy stored per unit volume. Viscous effects are neglected

filament plus its surrounding actin filaments (denoted as sarcomere subunit) depends on (1) the number of available cross-bridges n_{acb}, and (2) the average cross-bridge force under these conditions F_{cb0}. Parameter n_{acb} follows from the product of the number of myosin heads per unit length on the myosin filament λ, and the filamentary overlap f_1 of the actin filaments with the zone of myosin heads on one half of the myosin filament. Hence:

$$F_{cu0} = F_{cb0} \cdot n_{acb} = F_{cb0} \cdot \lambda \cdot f_1 \tag{1}$$

The subscript cu0 denotes the available cross-bridges (c) and zero interfilamentary velocity (u0). In vertebrates, λ is about 187 myosin heads/μm (Offer 1987). F_{cb0} was estimated to be 4.3 pN (Van Leeuwen 1991). In calculating f_1, four length ranges of the sarcomere are distinguished (Fig. 3a and b, curve I). The number of cross-bridges relates linearly to sarcomere length from $l_{act} + l_{myo} + l_z$ till $l_{act} + l_{bz} + l_z$. Further shortening results in a plateau in force production since the thin filaments slide over the bare zone. For short sarcomere lengths, corrections in the number of cross-bridges are needed owing to actin overlap between contra-lateral sides (for $l_{sarc} < l_{act} + l_z$) and collision of myosin with the Z-disc (for $l_{sarc} < l_{myo} + l_z$). This results in a further force decrease with sarcomere length (Fig. 3b, curve I). An algebraic expansion of f_1, based on experimental data of Gordon et al. (1966) and Edman (1979), can be found in Van Leeuwen (1991).

At short sarcomere lengths, passive forces (type one, F_{pas1}) arise from collision of the myosin filament with the Z-disc (if $l_{sarc} < l_{myo} + l_z$). Resistive forces owing to actin filament overlap (if $l_{sarc} < l_{act} + l_z$) play most probably a negligible rôle (Van Leeuwen 1991). These passive forces counteract the cross-bridge forces (i.e. act as power absorbents of the "cross-bridge motor"). They are represented by curve II in Fig. 3b. Algebraic expressions for F_{pas1} are provided in Van Leeuwen (1991).

The maximum active force F_0 of a sarcomere under isometric conditions and full activation (proportional to $l_{myo} - l_{bz}$ if $l_{act} \geqq l_{myo} - l_{bz}$) is often used to normalize the force components of the sarcomere. The familiar normalized force-length diagram is calculated as $(F_{cu0} + F_{pas1})/F_0$ (Fig. 3b, curve III). The sarcomere optimum length l_{0sarc} is defined as the centre length of the force plateau in Fig. 3b, curve III ($l_{0sarc} = 0.5l_{bz} + l_{act} + l_z$ if $l_{act} \geqq l_{myo}$).

Above optimum sarcomere length, forces act in parallel with the cross-bridges (type two passive forces, F_{pas2}; Fig. 3b, curve IV), resulting from tension in the connecting filament and tension in the sarcolemma (Podolsky 1964; Rapoport 1972). Tension in the sarcolemma changes presumably as a function of l_{sarc}, since it is connected to the sarcomeres via the T-system and via separate connections to the M-discs and Z-discs (Brown and Hill 1982; Street 1983; Wang 1985). Generally, at sarcomere strains below 0.1, F_{pas2} is negligible compared to the maximum active sarcomere force, except in insect flight muscles which have an exceptionally high passive stiffness (Sect. 4.2). An experimental recording of F_{pas2} is shown in Fig. 2 (denoted by "resting tension").

2.1.2 Force Production and Interfilamentary Velocity: Velocity Dependence Function

The interfilamentary velocity u is the velocity of the myosin filament with respect to its corresponding actin filaments. To follow the conventions from the physiological literature, u is chosen to be positive if the sarcomere shortens. Hence, the absolute contraction velocity of the sarcomere u_{sarc} is equal to $2u$. The relationship between the normalized average cross-bridge force and u is defined as:

$$F_u = (1 - u^*)/(1 + u^*/k) \qquad \text{for } u < 0 \tag{2a}$$

$$F_u = 1.8 - 0.8(1 + u^*)/(1 - 7.56u^*/k) \qquad \text{for } u > 0, \tag{2b}$$

where $u^* = u/u_{max}$, u_{max} is the maximum interfilamentary velocity for which force can be generated, and k is a constant which depends on the muscle fibre type (Otten 1987b). Formula (2) will be denoted as the velocity dependence function, a term introduced by Hatze (1981). This function depends only on u, whereas the force–velocity relationship, a term often used in muscle physiology and mechanics, depends not only on u, but also on sarcomere length and active state. Thus, a single force–velocity relationship for a muscle fibre does not exist. Edman (1979) showed that the externally unloaded maximum specific shortening velocity $\dot{\varepsilon}_{max}$ decreases linearly with sarcomere shortening for $l_{sarc} < l_{myo} + l_z$ (Fig. 2, V_0). Most probably, this decrease is caused by internal resistive forces owing to collision of myosin with the Z-discs. He showed also that $\dot{\varepsilon}_{max}$ increases above optimum sarcomere length. This is probably caused by a contribution of passive elastic forces (F_{pas2}). Nevertheless, formulae (2a) and (2b) are equal to formulae for the normalized force–velocity relationship from the literature, since at fibre optimum length the normalized force–velocity relationship should have a shape close to the velocity dependence function. Formula (2a) corresponds to the normalized Hill (1938) equation, whereas formula (2b) is based on Aubert (1956).

From the velocity dependence function, the mean normalized cross-bridge power can be obtained as a function of u, shown in Fig. 3d. With the selected k of 0.17, the maximum power output is found at $u = 0.276u_{max}$.

The usage of the velocity dependence function (although sufficient for the present purposes) has some limitations since measurements indicate that a long-term (hundreds of ms) force enhancement occurs after pre-stretch (Edman et al. 1978), while, during a forcible stretch, force is increased with sarcomere length (Granzier et al. 1989), probably caused by filament compression. The velocity dependence function cannot be used if very rapid step changes of length are applied to a muscle fibre as in the experiments by Huxley and Simmons (1971).

2.2 Muscle Fibre Activation

Muscle tissue is generally activated through nervous input, although mechanical activation occurs also in fibrillar flight muscles. Different types of innervation are found. Fast vertebrate muscle fibres are generally innervated by just one nerve fibre with one end-plate (see e.g. Vrbová et al. 1978). The nerve fibre may also

terminate with an array of end-plates (multiterminal innervation). Alternatively, muscle fibres may be innervated by several nerve fibres, each with several end-plates (polyneural and multiterminal innervation). This last type is found in many invertebrate muscles (e.g. Usherwood 1967), but is also one of the possible innervations in fish muscles (Bone 1978). It is thought that this type of innervation allows a more precise control of tension development in a muscle fibre. This seems to be especially important in very small muscles with a low number of muscle fibres. In mammals, a motor unit is the collection of muscle fibres being under control of one motoneuron. The nerve actionpotential is transmitted to the muscle fibre through release of a transmitter in the neuromuscular junction or synapse. Transmitter release causes a local depolarization of the sarcolemma (end-plate potential), which may lead to a muscle impulse transmitted along the membrane. The membrane generally has transverse invaginations known as the T-tubuli or T-system, which link the membrane to the sarcoplasmic reticulum (SR). Depolarization of the membrane causes a release of Ca^{2+} from the SR into the sarcoplasm which initiates contraction.

The mechanical response of a mucle fibre to a single nerve impulse is known as a twitch. Characteristics of the twitch are often used to make a functional distinction between different muscle fibre types. If nerve impulses follows each other with enough delay, a series of twitches is generated. If the delay shortens, twitches may partly or completely fuse to give a tetanus (Fig. 5a, c).

For the discussion of locomotor function it is convenient to have a mathematical description of the excitation-contraction coupling, enabling a simulation of twitch and tetanus. With some additions and alterations, the simple description formulated by Otten (1987b) is followed here. Quantitative details are provided in Appendix B. Following Ebashi and Endo (1968), the active state F_a is defined as the relative amount of Ca^{2+} bound to troponin. $F_a = 1$ if all interactive sites on the actin filament are exposed through the action of Ca^{2+}. In a resting muscle fibre, $F_a = F_{a0}$, so that $F_{a0} \leqq F_a \leqq 1$. Active force development is directly proportional to F_a.

2.3 Calculation of Force, Power and Work of a Muscle Fibre Under Dynamic Conditions

The average cross-bridge force of an activated sarcomere can now be described as the product of average cross-bridge force under isometric conditions and full activation, velocity dependence function, and active state: $F_{cb0} \cdot F_u \cdot F_a$. The dynamic force of the sarcomere F_{sarc} is equal to the sum of the cross-bridge forces and the passive forces:

$$F_{sarc} = n_{acb} \cdot F_{cb0} \cdot F_u \cdot F_a + F_{pas1} + F_{pas2} = F_{cu0} \cdot F_u \cdot F_a + F_{pas1} + F_{pas2}. \quad (33)$$

The work output W_{sarc} for a particular contraction from time t_a to t_b is described by:

$$W_{sarc} = \int_{l_{sarc}(t_a)}^{l_{sarc}(t_b)} F_{sarc}\, dl_{sarc}. \quad (4)$$

A solution of this integral is most conveniently obtained by numerical integration on a digital computer, since, during locomotor activities, both F_{sarc} and l_{sarc} vary in a complex way. Sarcomere power output P_{sarc}, the product of sarcomere force and velocity, is positive if force output and length change are in the same direction. Power output is negative when a muscle fibre produces force while it is stretched. In this case, energy is absorbed by the fibre.

For full activation ($F_a = 1$) and given values of l_{act}, l_{myo}, l_{bz}, l_z, a "force surface" is defined with the phase plane (l^*_{sarc}, u^*) as its base (Fig. 4a). Under all circumstances, force production of the muscle fibre is below this surface or just in this surface. Therefore, this surface may be called the "normalized force envelope" of the muscle fibre. Analogously, Fig. 4b shows a normalized power envelope. If $u^* > 0$, then power output is always below or just in the surface of maximum power. If $u^* < 0$, then power output is always above or just inside the surface. For both surfaces, F_{pas2} was neglected.

Figure 5a shows schematized twitch and tetanus responses of slow and fast muscle fibres of carp (Granzier et al. 1983). The above formulae may serve to simulate the twitch and the tetanus of a muscle fibre, as well as (more important) power output during dynamic circumstances as in locomotion. Figure 5c, left graph, shows twitch and tetanus simulations of a fast muscle fibre of the carp. Neither a "sag" phenomenon (i.e. a decline in tension during a tetanus, Fig. 5a) nor fatigue are incorporated in the model.

To investigate muscle fibre function in locomotion, it is very rewarding to measure the force output of isolated muscle fibres or small fibre bundles during length changes imitating in vivo strain variations. This technique was first developed by Machin and Pringle (1959, 1960) in their classical studies on the mechanics of asynchronous flight muscle. Quite recently, the technique has also been applied to synchronous insect flight muscle (Josephson 1985; Stevenson and Josephson 1990), frog sartorius muscle (Stevens 1988) and fish swimming muscles (Altringham and Johnston 1990). An example of a recording for fast twitch fibres of swimming muscles from a bullrout with a sinusoidal length change is shown in Fig. 5b. The work done in one cycle is proportional to the surface of the loop

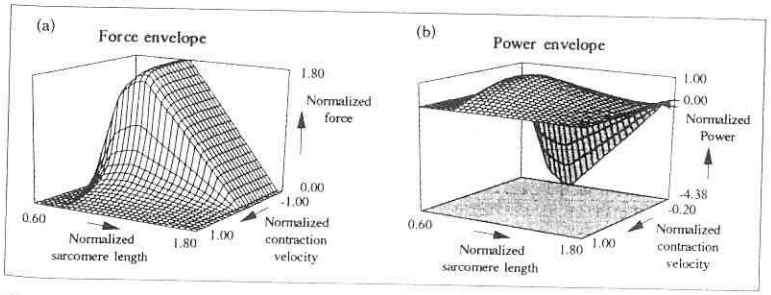

Fig. 4 a, b. Force (**a**) and power (**b**) envelopes as discussed in Sect. 2.3. *Small arrow* in **b**, *right side*, points to zero-power line through surface (along this line, the interfilamentary speed is zero)

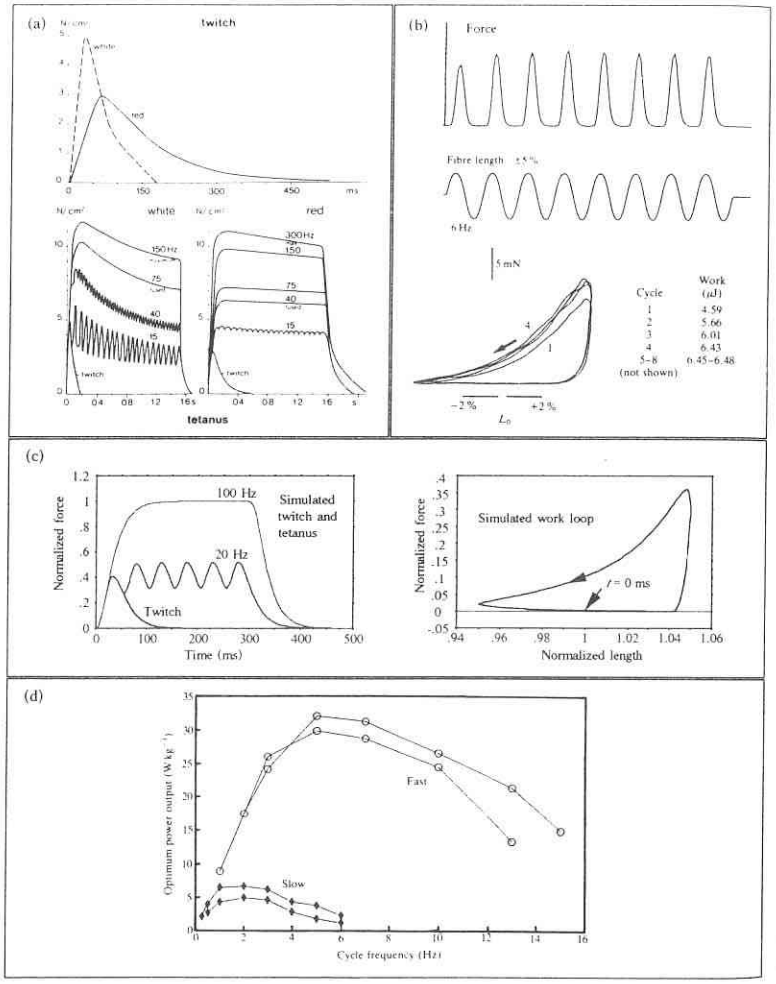

Fig. 5. **a** Schematized twitch (*top*) and tetanus (*bottom*) responses of slow (red) and fast (white) muscle fibre bundles of the carp (*Cyprinus carpio*), based on measurements from muscle-nerve preparation. (Granzier et al. 1983). **b** Measured force output of fast muscle fibres of a bullrout (*Myoxocephalus scorpius*) during a sinusoidal length change, and associated work loops (*bottom*). **c** Simulation of twitch and tetanus response for fast muscle fibre type (*left*, with stimulus frequencies as indicated), and work loop (*right side*, with a sinusoidal length change of $\pm 5\%$ about fibre optimum length, and one stimulus during stretching phase with phase angle of 54°). Parameters: $l_{act} = 1.75\,\mu m$, $l_{myo} = 1.57\,\mu m$, $l_{cbf} = 0.15\,\mu m$, $l_z = 0.06\,\mu m$, $\tau_{ca} = 6$ ms, $\tau_1 = 15$ ms, $\tau_{ca} = 20$ ms, $\hat{v}_{max} = 15$ lengths/s. **d** Power output as a function of cycle frequency for slow and fast fibres of bullrout (**b** and **d** Altringham and Johnston 1990)

obtained when force is plotted against length. A clock-wise loop denotes energy absorption (negative work), whereas an anti-clock-wise loop shows that positive work in done. Figure 5b shows measured work loops with one stimulus per cycle. Figure 5c, right plot, shows a simulated work loop of a fast carp fibre (one stimulus per cycle and comparative stimulus time). In all simulations of this chapter, it is assumed that all sarcomeres of a muscle fibre have equal lengths and activations. Thus, sarcomere strain is equal to muscle fibre strain. Work loops with different shapes are obtained if the activation characteristics are changed (Sect. 4.1; Figs. 16d, e, f). One advantage of a validated model of muscle fibre work output is that predictions can be made of in vivo muscle performances, guiding experimentation. Figure 5d shows a measured plot of the maximum mean power output against frequency for slow and fast muscle fibres of a bullrout. Fast fibres have a much higher peak performance but are more quickly fatigued.

2.4 Metabolic Cost Function

Muscle energetics is discussed in Chap. 8. A metabolic cost function will be introduced here since this helps to understand why muscles are active in particular phases of their lengthening-shortening cycles. Let $\hat{P}_\sigma$ be the metabolic power per unit volume of muscle needed to produce unit mechanical stress. $\hat{P}_\sigma$ is proportional to the length of the muscle fibre. The economy of a muscle is defined as $1/\hat{P}_\sigma$. Thus, relatively short fibres produce tension economically. Heglund and Cavagna (1987) measured tension of small leg muscles of a frog (*Rana esculenta*) and the rat at a range of contraction speeds. They recorded also the O_2 consumption of these muscles, allowing to estimate metabolic power. Close to $\hat{v}_{max}$, metabolic cost per unit force is about three times the cost at zero shortening velocity. Their experiment is somewhat hampered by the problem that the ratio of muscle belly speed over muscle fibre speed could vary, owing to the presence of tendinous sheets (see Sect. 2.7). Owing to muscle pennation, muscle fibres exert force against each other. Hence, strictly speaking, the results cannot be directly applied to a single muscle fibre. This problem is avoided if the experiment could be repeated with a single fibre or a small fibre bundle. Furthermore, slow fibres produce tension more economically than fast fibres. Loosely based on the experimental data by Heglund and Cavagna (1987) and a discussion by Woledge et al. (1985), the normalized metabolic power consumption for force production as a function of the interfilamentary velocity (Fig. 3e) can be described:

$$P^*_\sigma = 1.0 - 0.7(1 - u^*)/(1 + c_1 \cdot u^*) \quad \text{for } u^* > 0 \tag{5a}$$

$$P^*_\sigma = 0.1 + 0.2(1 + u^*)/(1 - c_2 \cdot u^*) \quad \text{for } u^* < 0, \tag{5b}$$

where $c_1 = 16$, and $c_2 = 160$ are constants. The specific metabolic power usage of a muscle fibre is obtained by:

$$\hat{P}_{met} = P^*_\sigma \cdot \hat{P}_{metmax} \cdot F_a \cdot f_l / f_{lmax}, \tag{6}$$

where $\hat{P}_{metmax}$ is the maximum specific metabolic power output and l_{lmax} is the maximum filamentary overlap. Formula (6) will be useful in the discussion of the dynamic properties of the muscle-tendon complex and muscle function in terrestrial locomotion.

2.5 Connective Tissue Properties

The connective tissue of a skeletal muscle belly is traditionally divided into three structural entities. The epimysium surrounds the whole muscle, the perimysium surrounds bundles of muscle fibres, whereas the endomysium surrounds individual muscle fibres. In isolated muscle fibres, the endomysium is considered to contribute significantly to the passive properties above sarcomere optimum length. Light et al. (1985) have shown that the amount of perimysium in a muscle is generally much higher than the endomysium content (dry mass ratio varied from 2.8 to 64 in different muscles). This indicates that, in an intact muscle, the contribution of the perimysium to passive elastic forces is very significant. Purslow (1989) showed the perimysium in bovine stermomandibularis muscle to be a crossed-ply arrangement of crimped collagen fibres which reorientate and decrimp on changing sarcomere length. Mean collagen direction with respect to the muscle fibres ranged from about 80° at $l_{sarc} = 1.1\ \mu m$ to about 20° at 3.9 μm. Purslow modelled the load-sarcomere length curve of the perimysium and showed good agreement with passive elastic properties of the muscle. He concluded that the rôle of the perimysial collagen network is to prevent over-stretching of the muscle fibre bundles above $l_{sarc} \approx 3.6\ \mu m$. Most likely, the endomysium works in a similar fashion. Therefore, in an activated muscle working around optimum sarcomere length, the contribution of the endo- and perimysium to force output can generally be neglected.

2.6 Scaling Effects, Optimal Design and Muscle Fibre Types

Sarcomeres operate at different frequencies in various locomotor systems. Using asynchronous muscle fibres, a small insect may operate its wings at a frequency of several hundreds of Hz, whereas the sarcomeres vary only about 2 to 3% in length during each wing beat cycle (Pringle 1972, 1975; Ellington, 1985). Cutts (1986) estimated sarcomere length changes of about 20% in flight muscles of zebra finches and budgerigars. For slow muscle fibres, Van Leeuwen et al. (1990) estimated sarcomere length changes of about 12% in continuously swimming carp. For kick-and-glide swimming, an estimate was made of about 20%. If the operation frequency of a sarcomere decreases, more time is available for each contraction. Hence, the sarcomere length change can be expected to increase so as to maximize the mean power output in a contraction cycle. Thus, for locomotor systems of large vertebrates, relatively large changes of sarcomere length may occur, owing to the low frequencies of movement. However, experimental data are still lacking. Alternatively, more muscle fibres of a slow type can be used to increase the efficiency and endurance (Goldspink 1977). Both strategies might also be used simultaneously.

The optimal design of sarcomeres was first discussed by Otten (1987a) who examined the work output in a full contraction of sarcomeres of different geometries. A more relevant optimization criterion was formulated by Van Leeuwen (1991). He modelled the effects of different sarcomere designs and contraction ranges on the specific myofibrillar power output. The mean specific power output by a sarcomere is determined by:

(1) The efficacy by which the available myosin heads are used throughout the contraction. Cross-bridges are lost owing to thin filament overlap and collision of the thick filament with the Z-discs. Power output is further diminished since the cross-bridges do work against an internal resistance (Sect. 2.1).
(2) The myosin head density in the sarcomere. The Z-disc and the bare zone on the myosin filament consume space and therefore reduce the cross-bridge density.

Theoretically, absolute maximum power output would be delivered by an ideal (but not feasible) sarcomere with parameters $l_z = l_{bz} = 0\ \mu m$ and $l_{act} = l_{myo}$, which makes an infinitesimal contraction at the interfilamentary contraction speed for optimum cross-bridge power. Figure 6a–d shows contour plots of the mean power output as a function of l_{myo} and l_{act}, calculated with Van Leeuwen's (1991) theory, and normalized with respect to the theoretical maximum. Each point on the power surface of Fig. 6a represent a separate simulation of a sarcomere contraction, starting at a sarcomere length of $1.5 l_{cmax}$ and ending at l_{cmax}, where l_{cmax} ($= l_{myo} + l_z$) is the sarcomere length with optimum cross-bridge density (Van Leeuwen 1991). The interfilamentary velocity u (set to $0.276 u_{max}$ for optimum cross-bridge power) was kept constant during the contraction and was defined to be equal for all sarcomere designs. Hence, the strain rate drops with increasing filament lengths. The power surface has a skewly oriented ridge with a virtually constant l_{myo}/l_{act} ratio (just below 0.8). The power output increases slightly along the ridge in the direction of greater filament lengths. The increase gets slower with longer filament lengths. These phenomena are explained as follows. If the ratio l_{myo}/l_{act} is kept constant, the strain rate is about inversely proportional to sarcomere length, whereas sarcomere force is roughly proportional to filament length. Thus, power output is only slightly affected. Proportionality is not exact since both l_{bz} and l_z were kept constant (at 0.15 μm and 0.06 μm, respectively). Hence, the slow power rise along the ridge is caused by an increasing cross-bridge density with longer filament lengths. The shorter the filaments, the larger is the effect on the power output of a change of filament length. Figure 6b is similar to Fig. 6a, but the contraction range is now decreased to only $0.03 l_{cmax}$. The l_{myo}/l_{act} ratio on the ridge is now about 1.

In locomotor activities, the dimensions of an animal and its surrounding medium (air, water or soil) determine roughly the range of operating frequencies and amplitudes of sarcomere contractions. Hence, the generation of a particular range of strain rates is required. Therefore, it is particularly interesting to prescribe the strain rate of the sarcomere contractions. The results for a large and a small contraction are shown in Fig. 6c, d. Now, a clear optimum is found, since increasing filament lengths require an increasing interfilamentary speed to keep the strain

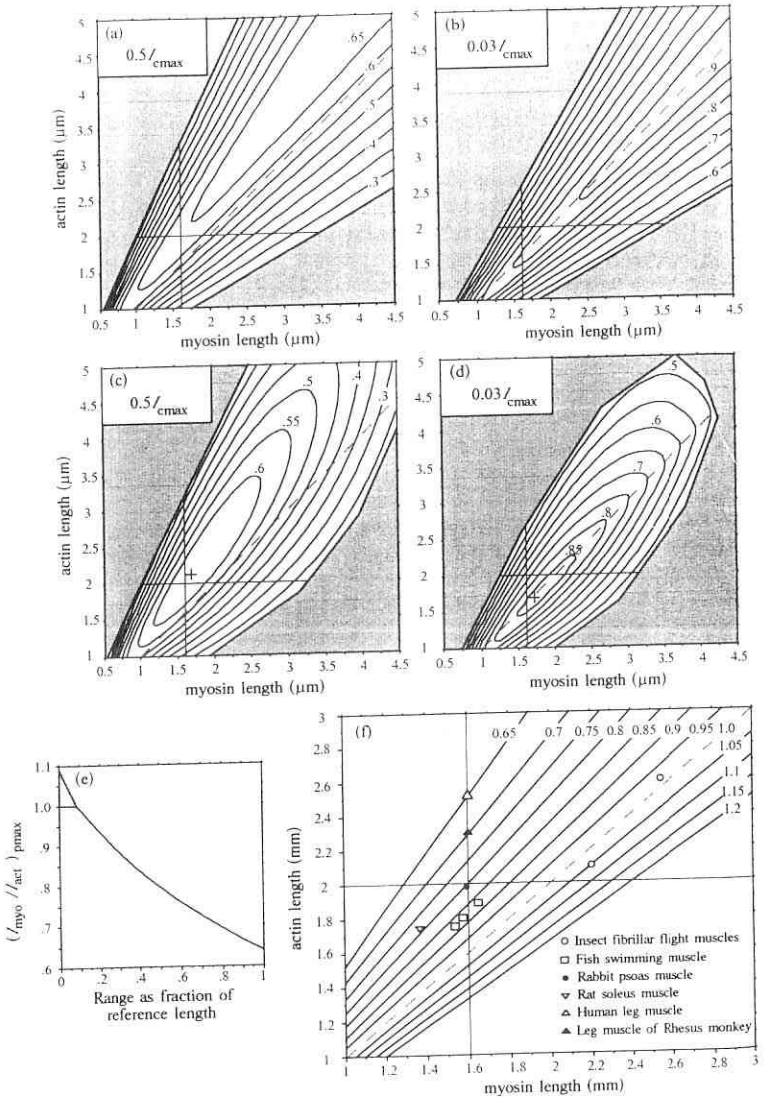

rate constant. Quite importantly, in the neighbourhood of each of the global maxima of Fig. 6c,d, power output is quite insensitive to changes in filament lengths if the ratio l_{myo}/l_{act} is kept constant. This is understood since close to the maximum in the normalized cross-bridge power function, the power drops only slightly with a changing interfilamentary velocity (Fig. 3d). However, the power output drops very rapidly if the filaments change length so as to alter maximally the ratio l_{myo}/l_{act}. This is caused by a drop in the efficacy of the usage of myosin heads during the contraction, owing to increased effects of only partial overlap between myosin and actin filaments or overlap of opposing actin filaments.

The position of the ratio l_{myo}/l_{act} for optimum power output, $(l_{myo}/l_{act})_{pmax}$, is shifted to a higher value if the contraction amplitude decreases (Fig. 6e). For a contraction from $1.5l_{cmax}$ to l_{cmax} (Fig. 6c) (still above the estimated amplitudes for some relatively small vertebrates, cf. Alexander 1989), the $(l_{myo}/l_{act})_{pmax}$ ratio is about 0.8. This ratio is "typical" for many small vertebrates. Fish use relatively small contraction ranges in continuous swimming, so that a relatively high (l_{myo}/l_{act}) is expected. This is supported by measurements (Fig. 6f). So far, however, only relatively small specimens have been investigated. It can be expected that very large fish use larger contraction ranges. For the very short range contraction of Fig. 6d (resembling the contractions of asynchronous flight muscles), maximum power output is found for a ratio of about 1. The $(l_{myo}/l_{act})_{pmax}$ value for a high amplitude contraction from $2l_{cmax}$ to l_{cmax} of 0.639 is very close to the lower limit of this ratio found till now in vertebrate sarcomeres (Fig. 6f).

In conclusion, the complete variation in the ratio of myosin length over actin length (from about 1.05 down to 0.65, as observed in insect and vertebrate sarcomeres, Fig. 6f) can be explained as a series of adaptations for optimum power output from a small to a large contraction range, respectively. Short contraction ranges with optimal design provide excellent peak power output (for fibrillar flight muscles about 0.9 of the theoretical maximum). Power output has a less steep sarcomere length dependence, but with a much lower mean specific myofibrillar power output, in an optimum design for a larger contraction. Using the above general theory, various predictions can be made. Two examples are (requiring further research): (1) During growth of an animal, the l_{myo}/l_{act} ratio will tend to decrease in most locomotor muscles (not necessarily in all muscles owing to

Fig. 6. Plot **a** shows contours of normalized mean power output $\bar{P}^*$ generated by a maximally activated sarcomere as a function of l_{myo} and l_{act}. Bare zone and Z-disc lengths were kept constant at the reference values (0.15 μm and 0.06 μm, respectively). The interfilamentary velocity was kept constant at 0.274 of the maximum. Values of $\bar{P}^*$ are given near a selection of the contours. The contraction range is $0.5l_{cmax}$. The reference sarcomere (with $l_{myo} = 1.6$ μm, and $l_{act} = 2.0$ μm) is positioned at the intersection of the *grey reference lines*. The *dashed skew line* represents $l_{myo} = l_{act}$. The *shaded areas* are of minor interest, and were not investigated. Plot **b** is similar to **a**, except that the contraction range is $0.03l_{cmax}$. Plots **c** and **d** correspond to **a** and **b**, except that now the strain rate is kept constant. Maxima are located at plus signs. Plot **e** shows the optimum l_{myo}/l_{act} as a function of contraction range. The *shaded triangle* indicates that a range of l_{myo}/l_{act} ratios gives optimum power under a particular contraction range. Plot **f** shows a scatter diagram of l_{act} against l_{myo} of measured sarcomeres from locomotor muscles (for references see Van Leeuwen 1991). **a** to **d** calculated using theory by Van Leeuwen (1991). **e** and **f** after Van Leeuwen (1991).

changing functional demands). (2) The expected large contraction ranges required for large birds limit, in combination with the low operating frequencies, the specific myofibrillar power output. This may help to explain why hovering flight (requiring, in birds, larger wing stroke amplitudes and sarcomere length changes than forward flight) is only used by insects and small birds.

Muscle fibres have been classified on the basis of structural criteria (innervation, mitochondrial content, structure of the SR, filament structure, etc.) and histochemical and biochemical criteria (e.g. abundance and efficacy of various enzymes). An overview of a variety of classification attempts for mammalian muscle fibres is given by Pearson and Young (1989). Functional criteria (endurance, contraction velocity, power output, twitch characteristics, etc.) are a useful guide for classification as demonstrated in a classical paper by Burke et al. (1973). Here, only a brief discussion from a mechanical viewpoint will be given with the aid of Fig. 7. For locomotion, specific power output by the muscle fibres is a dominant characteristic. A surface is drawn of peak specific power to visualize certain trends. No quantitative information can be extracted from this picture. Power output can be delivered in bursts, during long periods, or intermediate intervals. If sustained activity is required, than the local supply of metabolic power should cover continuously the mechanical power output (Weis-Fogh and Alexander 1977). For this purpose, an extensive battery of mitochondria is required, as well as an extensive system of blood vessels and, for insects, trachea for gas exchange and in- and output of metabolites. This apparatus requires space, which reduces the specific power output. Therefore, the power surface is lower at the right side of Fig. 7 than on the left side. The gain, however, is a relatively high mean specific power output. For optimal performance, the various components of the system of power supply and consumption should be tuned relative to each other, so that none of the components forms a limiting bottle-neck due to under design, or consume extra space by over design. This state of structural design whereby the formation of structural elements is regulated to satisfy but not exceed the requirements of the functional system has been denoted as symmorphosis by Taylor

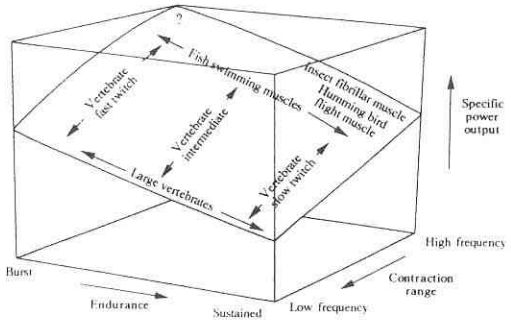

Fig. 7. Diagram used in a discussion of muscle fibre design and diversity. See text for explanation

and Weibel (1981). The specific myofibrillar power output increases if the contraction range decreases (see above). Therefore, the power surface increases from front to back. For sustained activities, the gain in specific power output from the sarcomeres by contraction range shortening is partially lost owing to increased space requirements for the energy supply apparatus. Therefore, the front-to-back slope of the power surface is steeper at the left side than on the right side. Another space-consuming structure is the SR, especially if fast response times are required as in synchronous insect flight muscles (5–20% of fibre volume, Ellington 1985). This negative effect on specific power output is largely overcome by the mechanically induced activation in asynchronous muscle fibres.

Muscle fibres designed for high power output during burst activities (fast twitch fibres, left side of power surface, Fig. 7) have a high myofibrillar content and a fast myosin-ATPase, whereas the energy supply apparatus consumes very limited space (during bursts, anaerobic metabolism prevails). Highest power output would be obtained if small contractions would be applied with appropriate sarcomere design and mechanical activation ("?" in Fig. 7). To my knowledge, this last option is not used in nature.

2.7 Dynamics of the Muscle–Tendon Complex

Muscle Architecture. The mechanical performance of a skeletal muscle is influenced by the geometrical arrangement of its muscle fibres (muscle architecture). A muscle is called parallel-fibred if its muscle fibres are parallel to the tendon(s) to which the muscle belly is attached. In pennate muscles, the fibres make particular angles with their tendon(s). Tendons do not stop abruptly at the muscle belly, but continue as tendinous sheets, to which bundles of muscle fibres (generally via a short collagenous tissue strap). The cross-sectional area of the tendinous sheet gradually decreases towards its end. This corresponds to a gradual decrease in the number of muscle fibres which can contribute to the mechanical load. Muscle fibre angulation influences the force output and length change (both vector quantities) of the muscle belly. This influence is variable, since fibre angulation increases during muscle belly shortening. Power and work output (scalar quantities) depend on muscle tissue volume, but not on muscle architecture (or only very slightly since internal energy losses may vary a little with architecture). Power output by the muscle-tendon complex (MTC) is the sum of the power output by the muscle tissue P_{mus}, the parallel elastic element in the muscle belly P_{par}, the tendinous sheets P_{ts}, and the tendons P_t. Models have been proposed to predict effects of architecture on force output and length change. Most models are planar and consider only straight muscle fibres. The considered models generally are kinematic abstractions, generally violating the force balance within the tissue. Classical papers on muscle architecture are by Stensen (Stenonis) (1667) and Benninghoff and Rollhaüser (1952) while Otten (1988) provides a recent review. All unipennate MTC models violate fundamental laws of classical mechanics. Some have an unexplained torque on the muscle belly, whereas others have an unexplained angle between tendon and tendinous sheets.

A Dynamic Muscle Tendon Model. Here, a planar model of a MTC with a bipennate muscle belly will be considered (Fig. 8), composed of straight muscle fibres, elastic tendons and tendinous sheets, and muscle volume V_m. The symmetry of the model avoids some problems of the unipennate model, but strictly speaking, curved fibres and tendinous sheets would still be needed. The inaccuracy of the present approach is small once the pennation angle is small or when the belly is long compared to muscle fibre length. For most muscles, these conditions are fulfilled. Let all muscle fibres have an equal pennation angle α, let they be of equal length l_f, let they have the same mechanical and activation properties, and let they have equal strain ε_f. The muscle fibres incorporate all quantified properties of Sects. 2.1 and 2.2. They can, in principle, be activated asynchronously, but only synchronous activations will be discussed. The pennation angle is α_0 if the muscle is at rest (i.e. not activated and not under tension). The length of the muscle belly is denoted by l_{mb}. The physiological cross-section of the muscle fibres A_{f0} equals V_m/l_{f0}, where l_{f0} is the resting fibre length. Furthermore, let the tendinous sheets have equal lengths l_{ts}, and let l_t be the total length of the tendons with slack cross-section A_{t0}. Let $l_{tts} = l_t + l_{ts}$ be the tendon length plus one tendinous sheet length. It will be assumed that equal strains ε_t act in the tendinous sheets and tendons, so that l_{tts} can be used as the effective length of the series elastic component. This assumption is supported by measurements by Rack and Westbury (1984) for low strains and by Morgan (1977) for high strains, although some doubts remain (Proske and Morgan 1987). The total instantaneous length of the MTC is given by:

$$l_{mtc} = l_{tts} + l_f \cdot \cos\alpha = l_{tts0} \cdot (1 + \varepsilon_t) + l_{f0} \cdot (1 + \varepsilon_f) \cdot \cos\alpha, \tag{7}$$

where l_{tts0} is l_{tts} at rest. Tendons and tendinous sheets (TTS) form the dominant components of the so-called series elastic element (SEC) of a MTC. From demands of constant volume it can be recognized that:

$$\alpha = \arcsin\left\{\frac{l_{ts0} \cdot l_{f0} \cdot \sin\alpha_0}{l_{ts} \cdot l_f}\right\}, \tag{8}$$

where l_{ts0} is l_{ts} at rest. The nonlinear stress–strain relationship of tendons and tendinous sheets used in the model (Fig. 3f) is loosely based on stress–strain

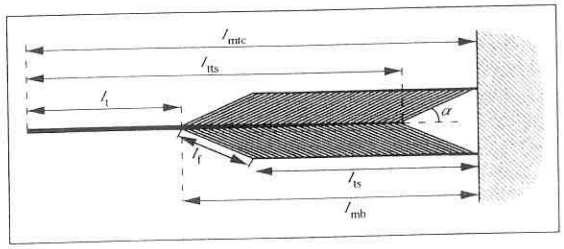

Fig. 8. Illustration of planar bipennate model of a muscle–tendon complex. Symbols are explained in Appendix A

measurements of tendons by Ker (1981) and Bennett et al (1986). Viscous effects are neglected since these are relatively small (only about 6% energy loss in cyclic movements). The stress–strain relationship (Fig. 3f) can be described by

$$\sigma_t = c_3 \cdot \varepsilon_t^{c_4} \qquad \text{for } \varepsilon_t < \varepsilon_c \tag{9a}$$

$$\sigma_t = c_5 \cdot \varepsilon_t + c_6 \quad \text{for } \varepsilon_t \geqq \varepsilon_c, \tag{9b}$$

where $c_5 = 1.5$ GPa (the tangent modulus), $c_6 = -22.5$ MPa, $\varepsilon_c = 0.035$ (the critical strain above which the relationship is linear), $c_3 = c_5/(c_4 \varepsilon_c^{c_4 - 1})$, and $c_4 = c_5 \cdot \varepsilon_c/(c_5 \cdot \varepsilon_c - c_6)$. The dominant viscous effects of the muscle belly are taken account of by the velocity dependence function [Eq. (2), Fig. 3c]. Inertial effects due to accelerations of muscle and tendon mass are neglected. In computing the force of the MTC (F_{mtc}), it was used that at any time tendon force (F_t) equals muscle belly force (F_{mb}). Hence, the instantaneous lengths l_f and l_{tts} and α can be found iteratively.

The above MTC model was implemented in a computer program, allowing to simulate effects on the mechanical performance of (1) different architectures (properties of tendons and tendinous sheets and muscle fibre properties like angulation, length and cross-sectional area), (2) different types (twitch, tetanus, etc.) and timing of activation. Furthermore, the model can be used to predict optimum architecture and activation for prescribed functional demands. Experimental observations can be used to check the validity of the model. On the other hand, the model can be used to reinterpret particular experiments or to design new ones. A small number of different simulations will now be discussed. The reference muscle architecture used is loosely based on the extensor digitorum longus muscle (EDL) of the rat, as described by Ettema and Huijing (1989). Muscle fibre characteristics are from Close (1964), after reinterpretation of his data (see below). The data are listed in Table 1.

Twitch and Tetanus. Figure 9 (left side) shows a simulation of the twitch response of a fast twitch muscle fibre in four different situations. In situation 1 (s1), the fibre

Table 1. Parameter values used in a simulation of a muscle–tendon complex (Figs. 9; 10a, b; 11 series 1; 12) Data are selected so as to loosely resemble the extensor digitorum longus muscle of the rat. Ultrastructural data from Van Lookeren Campagne et al. (1988), most architectural data from Ettema and Huijing (1989), and most physiological data from Close (1964), with slight changes. A_{t0} is assumed to be $A_{f0}/50$. Fibre angle α_0 is calculated from Ettema and Huijing (1989), but is probably slightly overestimated (see Close 1964). Symbols are explained in Appendix A.

Ultrastructural data:			
$l_{act} = 2.10\ \mu$m	$l_{myo} = 1.60\ \mu$m	$l_{hz} = 0.15\ \mu$m	$l_z = 0.06\ \mu$m
Architectural data:			
$l_{f0} = 11.78$ mm	$A_{f0} = 15.5$ mm^2	$l_{t0} = 18.94$ mm	$l_{ts0} = 20.95$ mm
$A_{t0} = 0.31$ mm^2	$\alpha_0 = 17^\circ$		
Physiological data:			
$\sigma_{miso} = 200$ kPa	$\tau_{ca} = 5$ ms	$\tau_1 = 5$ ms	$\tau_1 = 5$ ms
$\tau_s = 1$ ms	$f_s = 500$ Hz	$\hat{P}_{metmax} = 1000$ kW/m^3	

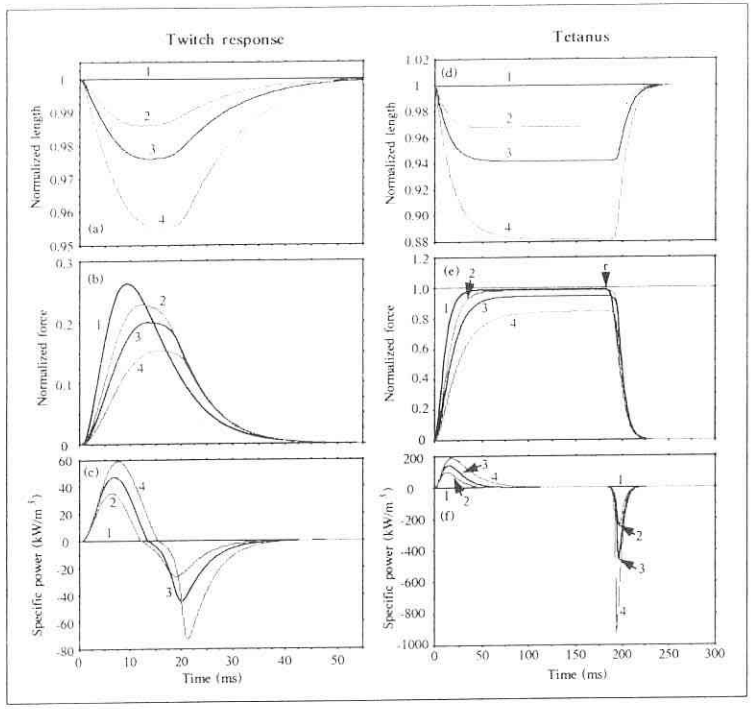

Fig. 9 a–f. Simulation of a twitch (*left side*) and tetanus response (*right side*) of *1* an isolated muscle-fibre kept at its optimum length, *2* the same fibre in a muscle belly of constant length, with tendinous sheets, but without a tendon attached, *3* the same fibre in a muscle belly with a tendon attached [reference MTC (Table 1) kept at constant length], and *4* the same fibre in a muscle belly with (compared to *3*) doubled tendinous sheet compliance, and quadrupled tendon compliance (cross-section 50%, length 200%). Muscle parameters of *1* to *3* are given in Table 1. **a** and **d** Normalized length of the muscle fibre. **b** and **e** Force production of the muscle fibre, normalized relative to maximum isometric force. **c** and **f** Specific power output of the muscle fibre. The *r* above the arrow in **e** denotes end of stimulus train

is isolated and kept at its optimum length. In situation 2 (s2), the fibre is part of a muscle belly with tendinous sheets, but without a tendon. The muscle belly is kept at the resting length, with muscle fibres at optimum length if no force is generated. Situation 3 (s3) is similar to 2, but now an external tendon is added. Situation 4 (s4) is comparable to s3, but with a doubled tendinous sheet compliance and a quadrupled tendon compliance (A_{t0} is halved and l_{t0} is doubled). The MTC is kept fixed at l_{mtc0}. As a result of the stimulus in s2 to s4, the muscle fibres shorten while producing force. The work done by the fibres is absorbed by the lengthening tendon (in s3 and s4) and tendinous sheets. Fibre length change

is fastest and largest in s4, since least force is required for a particular length change. During fibre shortening, force output of the fibre is reduced compared to s1, owing to (1) the velocity dependence function and (2) (small effect) the length dependency of activation. If, in the twitch, muscle fibre activation decreases again, fibre shortening still continues for a short time, since higher forces can be produced at a lower contraction velocity. Therefore, peak force of the muscle fibre is considerably delayed and reduced relative to s1. The peak becomes also much wider. This is true, even without an external tendon. In fact, in the simulated EDL, the tendinous sheets contribute more to the SEC than the tendon does, since they are longer. The effects of TTS compliance on force output are large, because force production is very sensitive to velocity changes if the interfilamentary velocity is close to zero (Fig. 3c). Therefore, it is also important, in physiological experiments, to reduce the compliance of the measurement equipment as much as possible. For the same reason, in mechanical models, it is important to include the nonlinear elastic properties of the TTS.

Owing to tendinous sheet lengthening, the muscle belly length tends to increase. This effect is compensated by extra muscle fibre shortening and rotation (compared to the situation with a non-elastic sheet). In contrast to the time to peak tension, the apparent relaxation time of the muscle fibres in s2 to s4 seems shorter than for the isolated fibre. This might explain the relatively low value of the half relaxation time (about 8.5 ms) as measured by Close (1964) for adult rat EDL as compared to the time to peak tension (about 12.5 ms).

Figure 9c shows the specific power output of the muscle fibre. The sum of the power of all muscle fibres in the muscle belly is equal in magnitude, but opposite in sign to the power output of the TTS (contribution of parallel elastic component is negligible). During muscle fibre shortening, muscle belly power output is absorbed completely by the TTS. During muscle fibre lengthening, the absorbed energy is released from the TTS in elastic recoil and absorbed again by the muscle fibres. Highest power output of the muscle fibres is produced in s4. Most metabolic power is consumed by the muscle tissue during the highest muscle fibre shortening velocities (not shown). During lengthening, metabolic power consumption is almost negligible.

In the tetanus (other conditions equal to those of the twitch, Fig. 9d, e, f), a similar delay in force production is observed for s2 to s4, but maximum force is reduced relatively less, since the shortening velocity goes to zero while the active state is still close to one. The final reduction is mainly due to cross-bridge losses. A minor effect is due to shortening deactivation. Naturally, muscle fibre shortening, force production, and maximum strain energy in the TTS are higher in the tetanus than in the twitch. The high magnitude of the negative power peak in de deactivation phase illustrates the high capacity of muscle tissue to absorb energy. The apparent relaxation (Fig. 9e) is delayed in s2 to s4, since stretching of the muscle fibres by the TTS during deactivation has a positive effect on force output. In conclusion, owing to the complex dynamics of the MTC, muscle fibre twitch and tetanus characteristics cannot directly be derived from muscle belly (or MTC) force measurements. The above observations are also relevant for locomotion studies (see Sect. 4.3 on terrestrial locomotion).

Force and Length. Simulation of a force length diagram of the MTC with full muscle fibre activation is shown in Fig. 10 (contraction speed → 0 m/s). Figure 10a shows F_{mtc} as a function of Δl_f, Δl_{mb}, and Δl_{mtc}, measured relative to the resting lengths. The force–length diagram is wider for Δl_{mb} than for Δl_f owing to (1) changing fibre angulation and (2) stretching of the tendinous sheets. The diagram is widest for Δl_{mtc}, since then tendon-length change contributes also. Optimum MTC force is exerted above MTC resting length, owing to (1) stretching of the TTS when force is produced, and (2) a decreasing pennation angle α with an increasing l_{mtc} (Fig. 10b), which favours muscle belly force output. Both effects are illustrated in Fig. 10c. Over the active force range, α varies from about 10° at

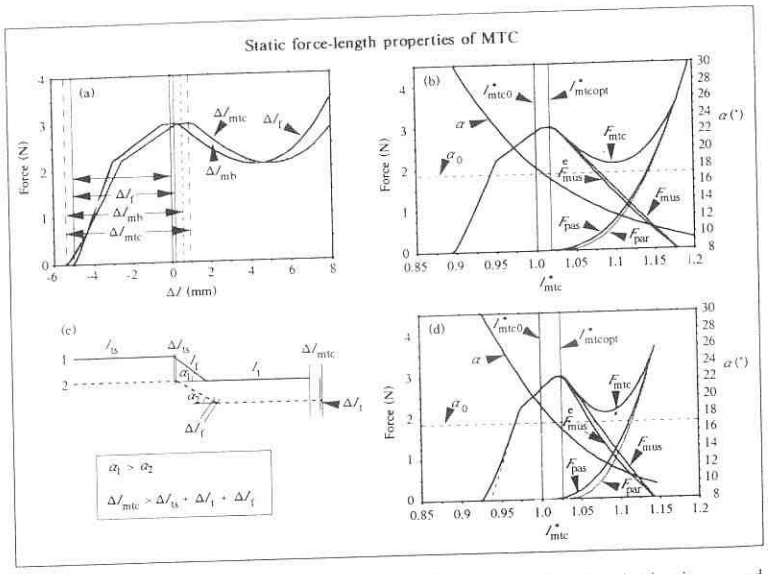

Fig. 10 a–d. Simulated static length tension characteristic of a MTC. Full activation is assumed. Muscle parameters are given in Table 1. In diagram **d**, however, l_{t0} was doubled, and A_{t0} was reduced by 50%. **a** Force output of MTC as a function of Δl_f, Δl_{mb}, and Δl_{mtc}, as denoted for each curve. *Vertical grey line* denotes position of zero length change with respect to resting value. *Other vertical lines to the right* denote excursion to optimum length, for the three length variables. Excursions are shown from minimum length till optimum length. *Unlabelled excursion* denotes value for isolated fibre. **b** Force output of the MTC F_{mtc}, of the muscle fibres F_{mus}, and of the parallel elastic elements F_{par} against normalized length of MTC. *Vertical grey line* shows position of l^*_{mtc0}. *Vertical line* shows l^*_{mtcopt}. *Horizontal dashed line* shows α_0. Passive length-tension curve of MTC is also shown: F_{pas}. The estimated muscle force (denoted with e) by subtracting the passive curve from the active curve deviates from the real muscle force, because F_{par} is smaller at a particular l_{mtc} when muscle fibres are active. **c** Diagram showing that in a pennate muscle a change in fibre length (from 1 to 2) is accompanied by a change in pennation angle so that $\Delta l_{mtc} > \Delta l_t + \Delta l_{ts} + \Delta l_f$. **d** Similar to **b**, but with a four times higher tendon compliance, and a doubled tendinous sheet compliance

maximum length to about 30° at minimum length, reducing muscle fibre force transmission by 12%, (but increasing transmission of length change) of the muscle fibres. Note that α changes fastest at shortest MTC lengths. Generally, the variation in α increases with an increasing α_0. Figure 10b shows also the separate contributions of the muscle fibres (F_{mus}) and the parallel elastic elements (F_{par}) to F_{mtc}. If the same length change is posed upon the MTC, but with inactive muscle fibres, the so called passive length–tension diagram is obtained (Fig. 10b: F_{pas}). In experimental practice, the active length–tension diagram is often obtained by subtracting F_{pas} from F_{mtc}. As discussed by Zajac (1989), this is principally incorrect, because, at the same MTC length, the parallel elastic structures are at a longer length during passive force measurements than when the muscle fibres are active (active muscle fibres cause an extra stretch of the TTS). This effect increases with the compliance of the TTS, as shown in Fig. 10d, with a doubled tendinous sheet compliance and a quadrupled tendon compliance. The situation of Fig. 10d is by no means exceptional for locomotor muscles. The rapid change in slope at the ascending limb of the force–length diagram (Fig. 10b, d) corresponds to collision of the myosin filaments on the Z-discs at short lengths. The lower part of the ascending slope is not straight (compare with dashed line in Fig. 10d) owing to variation of both α and TTS-length. A variation of muscle fibre properties may further increase this effect. The demonstrated salient features of the simulated force–length diagram are supported by measurements on cat soleus muscle by Rack and Westbury (1969) and various leg muscles of the cat by Poliacu Prosé (1985).

MTC Mechanics During Sinusoidal Length Variation. The above simulations of MTC mechanics are representative for many physiological measurements. During locomotor activities, however, muscle fibre activation and l_{mtc} change simultaneously. A convenient way of demonstrating the dynamic properties of the MTC is by prescribing a sinusoidal change of l_{mtc} around l_{mtc0} (Fig. 11b), and calculating the effects on force and power output. The MTC can only absorb power (i.e. produce negative power) when it is forcibly stretched, whereas it produces only positive power when it shortens. Muscle parameters resemble again those shown in Table 1, except that the TTS stiffness is increased (10 times) in series 2 of Fig. 11 and decreased (2 times) in series 3. Oscillation amplitude is ±2.5% of MTC resting length, with a frequency of 10 Hz. The contribution of the parallel elastic element was totally negligible and therefore omitted in Fig. 11. The contributions of the tendon and the tendinous sheets will be summed. In fact, the contribution to stretch and strain energy uptake is slightly larger for the tendinous sheets than for the tendon, owing to their slightly longer length. The cycle starts at minimum MTC length, so that the MTC is stretched during the first half of the cycle. Activation was by a 500 Hz train of 24 pulses, delayed by 28 ms relative to the start of the cycle. The first cycle differs slightly from subsequent cycles, owing to a small transient effect. The choice of parameters was guided by electromyographic records from the literature and the goal of demonstrating the salient dynamic features of the MTC. No special effort was made to find optimal conditions for particular functional demands.

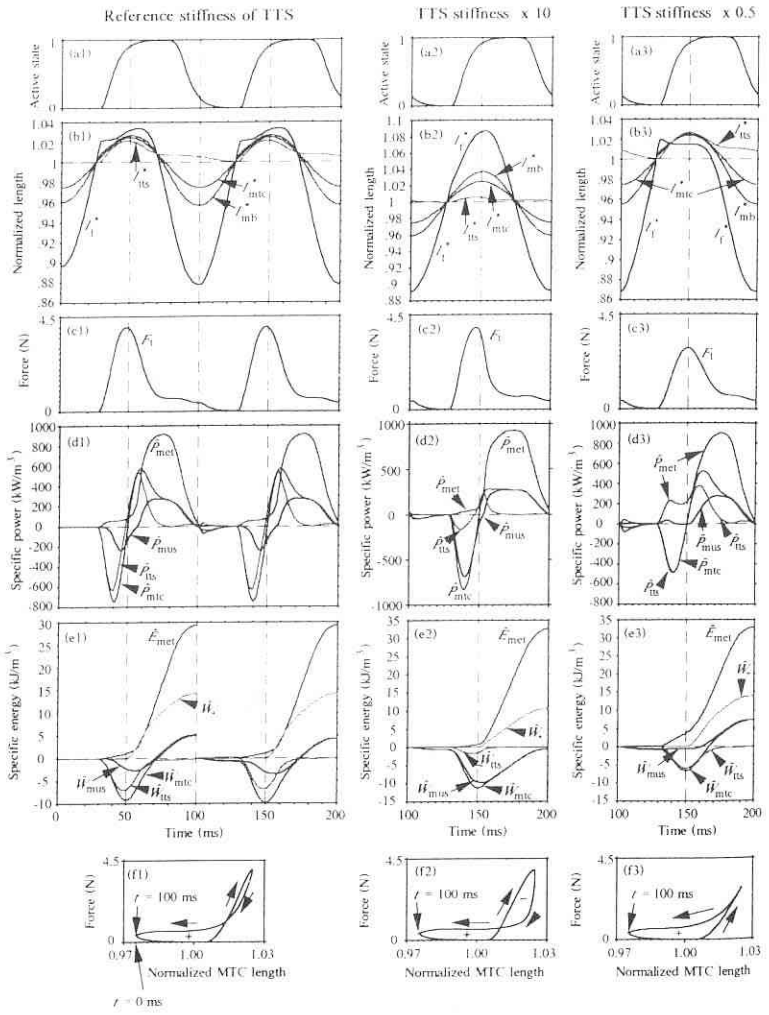

Fig. 11 a–f. Simulation of the dynamic response of a muscle–tendon complex (MTC) to a prescribed sinusoidal length change around resting length l_{mtc0} (peak-to-peak 5%). Plots **a1** to **f1** show results for the reference MTC of Table 1. Two subsequent length-change cycles of 100 ms each are examined. The length cycles start at minimum length. **a1** Active state as a result of 24 pulses at 500 Hz, started with a delay of 28 ms. **b1** Normalized length changes of MTC (l^*_{mtc}), muscle fibres (l^*_f), tendon and tendinous sheets (l^*_{tts}), and muscle belly (l^*_{mb}). **c1** Force production by the MTC. **d1** Specific mechanical power output of muscle tissue ($\hat{P}_{mus}$), TTS ($\hat{P}_{tts}$), and MTC ($\hat{P}_{mtc}$), as well as the consumed metabolic power ($\hat{P}_{met}$). **e1** Specific work and metabolic energy as obtained by integration of curves in **d1**. Energy levels are reset to zero at start of each cycle. The positive work done during the shortening period of the MTC is also shown ($\hat{W}_+$). **f1** Work loop of the MTC during the two cycles. Positive part is larger then negative part. Plots **a2** to **f2** are equally arranged as **a1** to **f1**, but now with a ten fold stiffer TTS, and only the second cycle is shown. Plots **a3** to **f3** show simulation results with a doubled TTS compliance (compared to series 1). Again, only the second cycle is shown

The active state rises almost to peak level during the stretching phase (Fig. 11a1); during most of the shortening phase it has a high level, but it is again close to zero at the end of the cycle. The normalized length changes of various parts of the MTC are shown in Fig. 11b1. The amplitude of normalized length change is largest in the muscle fibres. Under their optimum length, they follow a path close to a sine wave (a spectral analysis would allow a more exact statement). However, upon activation during stretching, the fibres quite abruptly reduce their speed and deviate from the sinusoidal path. Fibre length change is limited owing to force production (Fig. 11c1), so that MTC length change is largely due to stretching of the TTS (Fig. 11b1). The energetic effect is a high power absorbency by the TTS (which is stored as elastic energy) and a relatively low power absorbency by the muscle fibres (Figs. 11d1 and 11e1). Peak MTC force is produced before peak MTC length, since muscle fibre velocity drops towards the end of the stretching phase. Therefore, the TTS starts shortening before MTC shortening. Hence, muscle fibre velocity is opposite to TTS velocity. This situation continues for about 7 ms during the shortening phase. Thus, released TTS strain energy is absorbed during a short period by the muscle fibres. Although it is not shown by the simulation (it is not incorporated in the model), part of this absorbed energy could again be stored as elastic energy in the cross-bridges, since muscle fibre length change is only about 1%, which is below the limit of 3% for effective storage (Flitney and Hirst 1978). In fact, during the whole forcible stretching of the muscle fibres, the length change remains within this limit. Although the storage of strain energy in cross-bridges is a relatively small effect, it seems nevertheless useful in the transition from MTC stretching to shortening. Most TTS strain energy is released during muscle fibre and MTC shortening (first half of shortening phase). This energy shows up directly as MTC power output. The positive power output by the muscle fibres is delayed relative to this strain energy release. Thus, in the first phase, MTC power output (P_{mtc}) is dominated by strain energy fluctuations of the TTS and, finally, by muscle tissue power output. Most muscle fibre work is done at a relatively low force level. Metabolic power requirements are low during the stretching phase, and increase sharply when the muscle fibres start shortening. The MTC work output (W_{mtc}) produced during a complete length cycle can be divided by the total metabolic energy consumed per cycle to obtain an overall efficiency of 14.7% for this case. The total specific work output by the MTC during the shortening phase only ($\hat{W}_+$) is about 50% of the total metabolic energy. The work loop (Fig. 11f1) has a small negative part and a dominant positive part.

The simulation shows that the muscle fibres are mainly active at and below their optimum length for force production. This agrees with estimated sarcomere length changes in vertebrate locomotion muscles (reviewed by Alexander 1989),

and provides a high specific power output of the sarcomeres by increasing the cross-bridge density (Van Leeuwen 1991).

Now, the above simulation will be compared with the situation of a tenfold increase of the TTS stiffness (Fig. 11a2–11f2), whereas other parameters are kept constant. Only the second cycle is shown. The most conspicuous differences are:

1. Muscle fibre length follows much more the sinusoidal length variation of the MTC above resting length, leading to an increased sarcomere excursion, particularly towards higher lengths. This is caused by the more limited stretching possibilities of the TTS.
2. A faster force increase during lengthening, owing to a faster muscle fibre lengthening. Peak force falls earlier. During MTC shortening, the force decreases faster, owing to the higher muscle fibre shortening speed.
3. A much higher power uptake by the muscle fibres during MTC stretching, combined with a very limited strain energy storage by the TTS (Fig. 11d2, e2). MTC power output is now dominated by the muscle fibres.
4. MTC work output in the cycle is slightly negative, resulting in a slightly negative efficiency (-1.7%). This is also shown by the MTC work loop with about equal negative and positive parts (Fig. 11f2).

More or less reverse effects occur when TTS compliance is doubled with respect to the reference values (Fig. 11a3–11f3):

1. With the onset of activation, muscle fibres start to shorten slightly, until a plateau is reached (Fig. 11b3). The TTS is lengthened more than the reference TTS.
2. A lower peak force is reached, since muscle fibres are not stretched. Peak force coincides with peak MTC length. Force decline is relatively slow during MTC shortening, since, for most of the time, the muscle fibres shorten slower.
3. Power absorption during MTC lengthening is almost completely due to TTC strain energy uptake. Thus, power absorption by muscle fibres is almost completely avoided by doubling the TTS compliance.
4. MTC work output in the cycle is positive, with an efficiency of 22.2% (7.5% higher than for the reference MTC). The work loop shows a positive part only.

A muscle action like that of Fig. 11 series 3 is particularly useful in saving metabolic energy when, during locomotion, an animal makes cyclic changes in kinetic and potential energy (Sect. 4.3). It demonstrates also how, by an activated prestretch, muscle performance during MTC shortening can be improved, by making effective usage of the build-in springs of the muscle. For a jump from stant still, this requires a preceding counter-movement.

In real live situations, often only a particular fraction of fibres of a muscle is activated. Compared to a full activation, these fibres "see" a relative stiff TTS. This is roughly similar to a full activation with a very stiff TTS (Fig. 11 series 2). A small fraction of active fibres, particularly if distributed over the muscle, is unlikely to be able to take much advantage of elastic effects, which will reduce the efficiency. If the fraction of active fibres is localized, a higher efficiency can be obtained, owing to a greater stretch of the associative tendinous sheet parts. The low

efficiency can (partly) be compensated by usage of slow oxidative fibres during slow movements. The consequences for the co-ordination of muscle activities during locomotion will be further discussed in Sect. 4.3.

A high muscular efficiency is not always desired. If an animal wants to brake its movements suddenly, it needs a very low (i.e. high negative) efficiency. The timing of the activation has a dominant influence on the MTC power output. Figure 12a1 to 12c1 shows a simulation with an early activation (starting at 0 ms) in the stretching phase, resulting in a high power absorption by the MTC and a large negative work loop. Such activation would be useful if an animal wants to decelerate rapidly. Figure 12a2 to 12c2 shows a simulation with an activation starting at 40 ms, resulting mainly in positive power output by the MTC and a positive work loop. Such activation is useful if a high acceleration is required. The simulations demonstrate that muscles are particularly good in absorbing large amounts of work.

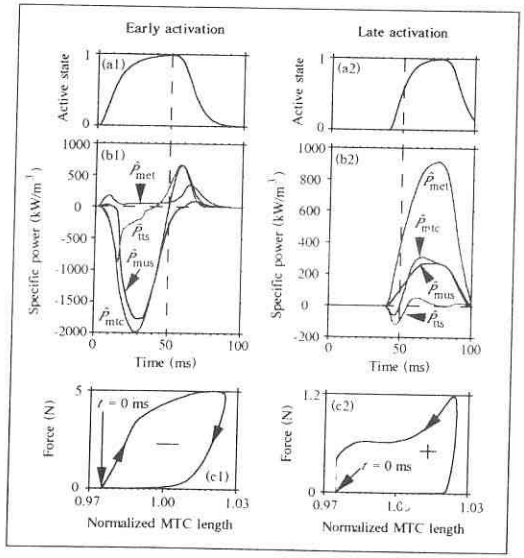

Fig. 12a–c. Simulation of the dynamic response of a muscle–tendon complex (MTC) to a prescribed sinusoidal length change around resting length l_{mtc0} (peak-to-peak 5%). The reference MTC of Table 1 is used. Duration of cycle is 100 ms. The cycle starts at minimum MTC length. The effect of different phases of stimulation on the power output is demonstrated. Series **1** shows an early activation, resulting in a high power absorption by the MTC. Series **2** shows a late activation, which produces a high power production. **a1** Active state as a result of 24 pulses at 500 Hz, started at $t = 0$ ms. **a2** The same but activation starts at $t = 40$ ms with only 18 pulses. **b1** and **b2** Specific power output of MTC components and specific metabolic power, labelled as in Fig. 11d. Absolute peak value of peak power absorption of MTC in **b1** is much higher than peak power produced in **b2**. **c1** and **c2**. Work loops. *Arrows* on curves show direction of movement. In series **2**, the loop is not closed since the fibres are still active at the end of the cycle

In conclusion, a TTS with appropriate stiffness can increase considerably the mean MTC power output. Using the present dynamic MTC model, the required stiffness and stimulus characteristics for optimization of power output and muscle efficiency under particular functional demands can be predicted.

Measurements of MTC Mechanics. Heglund and Cavagna (1987) recorded the work output of the EDL of the rat, and estimated also metabolic power from O_2 consumption measurements. They found that $\hat{W}_+$ could be increased if a forcible pre-stretch was given to the EDL as compared to an initially isometric EDL. This can mainly be explained as follows. The work done on the preparation during stretching was partly stored as strain energy in the tendinous sheets (Heglund and Cavagna excluded the main part of the external tendon, but the tendinous sheets are of about equal importance as the external tendon in the EDL), which was again liberated during shortening. The authors measured negative work loops for the complete cycle, so that the overall efficiency of the MTC was negative. (The conclusion of Heglund and Cavagna that the efficiency of the EDL was increased by the pre-stretch was based on a misconception that the efficiency could be obtained by dividing $\hat{W}_+$ by the used metabolic energy). This experiment was important since it supports the view that previously stored strain energy can contribute importantly to power output during MTC shortening. If a MTC is pre-stretched, the series elastic component is relatively longer at the time of transition from lengthening to shortening as compared to an initially isometric MTC. At the same time, the muscle fibres are relatively shorter. Hence, on average, a lower contraction speed of the muscle fibres results during MTC shortening, which leads, according to the velocity dependence function, to a higher force output. The difference in contraction speed will be highest during the initial phase of shortening, which indeed shows the highest measured force enhancement (Cavagna et al. 1968). Simulations with the present model (using constant stretching and shortening velocities) showed this effect to last for about 30 to 40 ms during shortening. Cavagna et al. (1968) suggested that yet another effect on the contractile apparatus would be present owing to (1) the considerable duration of force enhancement (several hundreds of ms) and (2) the presence of a (slight) force enhancement, even if a 20 ms isometric phase was between the pre-stretch and the shortening phase. Firm support for this suggestion came from measurements on isolated frog muscle fibres by Edman et al. (1978). This last, yet to be defined, effect of the pre-stretch is not incorporated in the present model.

Heglund and Cavagna (1987) showed that the pre-stretch effect was much less for frog sartorius muscle than for rat EDL. A likely explanation is that the sartorius is parallel fibred muscle (one of the very few) with very short tendinous sheets, so that very little strain energy can be stored in them. In cat (Loeb et al. 1987) and man (Barrett 1962), the muscle fibres do not run continuously throughout the muscle belly, but the muscle fibres are connected to each other in series with short strips of connective tissue.

Just before this chapter was finished, an experimental study by Ettema et al. (1990) on rat medial gastrocnemius muscle was published which shows several of the phenomena discussed in this section.

3 Monitoring Muscular Performance in Vivo

This section considers methods used to record muscle performance in vivo. Direct measurements can be made of muscle performance (Sect. 3.1), or models can be used to estimate muscle performance from experimental data as external force records and cinematography (Sect. 3.2). Sometimes combinations of the two approaches are being made (Sect. 3.3).

3.1 Direct (Invasive) Experimental Techniques

Electromyography. The electrical activity of muscles can be measured by electromyography (EMG). Details about the technique can be found in textbooks on electrophysiology. For muscle function in locomotion, the differential technique gives the best results, since it allows a localized registration of muscle activity. Here, two identical electrodes are positioned closely together and the difference in potential between them is recorded. Surface electrodes have limited resolution, but are, for obvious reasons, often used in recordings from man. Needle and wire electrodes have the advantage of a higher spatial resolution. Generally, EMGs give only an impression of electrical activity, they do not show how much force is being produced. Force production lags behind electrical activity. For fast muscle fibres, the delay is about 20–30 ms, for slow fibres it is about 50–80 ms. Many attempts have been made to relate EMG to force output. For isometric cases, the rectified and low pass filtered EMG has been shown to be roughly proportional to force output. If length changes are involved, the situation is more complex. Hof and Van den Berg (1981) predicted force output of the human calf muscles, using an adaptation of the muscle model by Hill (1938). A disadvantage of their approach (and those of many others) is that (1) the muscle parameters have limited structural or physiological relevance, and (2) a calibration technique is required, since electrode placement is highly variable.

Direct Force Measurement. An important technique to measure force from a single muscle or from a muscle group with a common tendon is by the usage of a tendon buckle transducer (first proposed by Salmons 1969). This technique is limited to muscles with relatively long tendons, being exposed to surgical approach. The Achilles tendon is used most frequently. The technique has now been applied by several investigators. Early studies were by Barnes and Pinder (1974) in the horse and Walmsley et al. (1978) on cat Achilles tendon. Sherif et al. (1983) compared myoelectrical activity and muscle force during running in the cat. Biewener et al. (1988) used the tendon buckle technique to measure forces by the ankle extensors in hopping kangaroo rats. They showed that the entire range of possible muscle forces is used during normal locomotor events. At slow speeds: 20% of the maximum isometric force; at preferred speed 40% and during jumps 175% during the stretching phase of the muscles. Peak muscle stresses were found of about 350 kPa.

Direct Strain Measurement. Mercury tubes have been used to measure the strain of tendons during locomotion of the horse, using the property of a changing electrical

resistance during lengthening and shortening (Van den Bogert et al. 1989). Muscle forces and elastic energy storage can be calculated if, after in vivo experimentation, the tendon properties are measured with a tensile testing machine.

3.2 Indirect Techniques

Muscle performance can be estimated with various indirect (noninvasive) techniques. Almost all methods require knowledge about muscle moment arms and muscle architecture. So, these aspects will be discussed first.

Moment arms. There are various ways to estimate muscle moment arms (An et al. (1984) provide a review). Morphometry can be applied if the position of the motion axis of the joint can be simply correlated with a curved joint surface in the specimen. If motion axis and force are at right angles, the moment arm equals the distance from axis to muscle-tendon complex (along the common perpendicular). This approach becomes problematic when the motion axis cannot be easily related to the skeleton. Axis and tendon position can be accurately determined by Röntgen photogrammetry (Selvik 1990), but this technique is laborious and often not available. Moreover, tendon constraints like retinacula and tendon sheaths can hinder the determination of the line of action of the tendon force (An et al. 1984). A muscle moment arm as a function of joint angulation $r_m(\phi)$ can be most simply and most accurately obtained from measurements of tendon displacements s as a function of ϕ in a musculoskeletal preparation. By assuming that, in an infinitesimal displacement, the work done by tendon displacement is equal to the work done by the muscle in the joint rotation (principle of virtual work), the moment arm r_m is calculated (An et al. 1984):

$$F_t \mathrm{d}s = F_t \cdot r_m \mathrm{d}\phi. \tag{10}$$

Hence:

$$r_m = \frac{\mathrm{d}s}{\mathrm{d}\phi}. \tag{11}$$

The same relationship can be derived by a kinematical analysis for planar motion (Fick and Weber 1877; Brand et al. 1975). The main advantage of this technique is that it takes implicitly account of complex joint geometries, curved muscle paths and three-dimensional effects. If neglects, however, stretching effects of e.g. a retinaculum. Measurements of moment arms of human lower leg muscles about knee and ankle joint, using this technique, show the arms to be quite variable (Spoor et al. 1990), so that considerable errors can be made about muscle function if a constant moment arm is assumed.

Muscle architecture. Muscle architecture is still obtained best from dissections. Measurements include the following:

1. Tendon mass, slack length and cross-sectional area.
2. Slack length and mass of tendinous sheets.

3. Lengths and pennation angles of muscle fibres (or small bundles) should be measured evenly spread over the muscle belly.
4. Muscle volume and fibre cross-sectional area.
5. Sarcomere lengths of each of the dissected muscle fibres. (This can be done with a diffraction method. A cheap and convenient method is described by Dimery 1985).
6. Sarcomere structural parameters (by electron microscopy).

These structural parameters are required as input for a muscle-tendon model (Sect. 2.7). From measurements (3), (5) and (6), the muscle fibre optimum length can be calculated. Additional experiments are required to obtain physiological data. A diffraction method can also be used to estimate sarcomere lengths during a locomotor activity (Dimery 1985; Cutts 1986). To this end, killed animals are placed in positions corresponding to those from a film of the moving animal. The method is only approximate, since in vivo force patterns differ with an unknown amount from rigor forces of the muscles. If joints are well characterized, motion data can sometimes be used to calculate MTC length changes (Van den Bogert et al. 1989).

Inverse Dynamics Analysis. Muscle forces can be estimated using the so-called inverse dynamics approach (mathematical details and computer methods of this technique are described in engineering textbooks like Haug 1989). In this approach, net joint moments are calculated from

1. measured (by cinematography or accelerometry) positions, velocities and accelerations of the body segments (kinematic analysis);
2. inertial parameters of body segments.

The net joint moments are subsequently used to estimate muscle forces with the following additional information:

1. instantaneous moment arms of muscles and ligaments about the various joints;
2. muscle and ligament properties;
3. a (validated) distribution model for the forces over the concerned muscles and ligaments.

The pitfalls of this method are manifold. (1) The estimation of accelerations from noisy displacement data (owing to e.g. unwanted displacements of skin markers) easily leads to significant errors. Special computational techniques have been developed to reduce these errors as much as possible (e.g. Woltring 1986). (2) Body segments are often assumed to be rigid. (3) Moment arms are generally only poorly known. They can be quite sensitive to joint angulation (Spoor et al. 1990). (4) Presently available force distribution models are based on arbitrary principles. The best load sharing model for muscles to date seems to be the minimum fatigue criterion by Dul et al. (1984). This criterion is based on the assumption that the endurance time of muscular contraction is maximized, hence muscular fatigue is minimized. A better criterion, incorporating the dynamic properties of the MTC (including both muscle fibre types and elastic properties), will be discussed in Sect. 4.3.

Terrestrial locomotion studies often use force platforms to measure ground reaction force on the feet of the animal. These forces can be used to estimate muscle forces, if the following additional information is available:

1. Instantaneous moment arms of reaction forces, muscles and ligaments about the various joints.
2. Muscle cross-sectional areas and ligament properties.
3. A (validated) distribution model for the forces over the concerned muscles and ligaments.
4. A multi-body model of the animal to account for segmental accelerations.

In practice, ligament forces and segmental accelerations are often neglected, whereas equal stresses are assumed to act in synergistic muscle groups in combination with inactive antagonists. This last assumption is not generally acceptable (Sect. 4.3). This approach generally saves much computational effort, whereas the accuracy is generally better than with a purely inverse dynamics approach. Nevertheless, at the end, only an order of magnitude estimate can often be made for the muscle forces. Biewener et al. (1988) compared the indirect approach to estimate muscle forces with results from the tendon buckle technique. Predictions of peak forces corresponded quite well. At low force levels, relatively large differences were found.

Direct Dynamics Analysis. In a (direct) dynamics analysis (e.g. Hatze 1981), the motions of the body segments are calculated from the driving forces of the muscles, controlled by neural inputs. Basic computer methods for the engineering aspects of this analysis can be found in e.g. Haug (1989). The method is attractive, since it follows the same route as the body does (naturally, the body uses also sensory information). As a check of the model validity, calculated body segment trajectories can be compared with measured trajectories (Otten 1987b). Generally, however, the method is still hampered by the large numbers of parameters, numerical difficulties and oversimplifications owing to many unknown or ill defined factors. Modern image analysis techniques may help to reduce the number of structural unknowns (Otten 1987b).

Combined Techniques. Sometimes, it is desirable to follow a combined approach. Using the inverse dynamics analysis, net joint moments can be calculated for a moving animal. These moments can be used as input for a direct dynamics model, except for one joint which could be controlled by models of muscle-tendon complexes. Effects of parameter variation for one joint on the movements and reaction forces of the whole animal can then be studied.

4 Performance and Design of Muscles in Some Locomotor Systems

4.1 Fish Swimming Muscles

Considerable progress has been made in the understanding of fish swimming muscles in the last decade. Therefore, this topic will be discussed at some length. Fish use a great many different techniques to propel themselves. In one swimming type, the body is propelled by undulatory movements of the fins, whereas the body is kept relatively rigid. A further subdivision can be made on the basis of the relative contributions of each of the paired and unpaired fins. These swimming modes are generally used if a high efficiency is required. The dominant type of swimming is by undulation of the body, the main topic of this section. This swimming type can further be divided in three distinct modes. (1) In continuous swimming, the body repetitiously makes undulations of fixed amplitude and frequency. (2) In kick-and-glide (= intermittent) swimming, body undulations are intermitted with glides, with the body kept straight. Now, an acceleration phase can be distinguished from a deceleration phase with no power output from the trunk muscles. (3) In a fast start, the body is accelerated from rest by undulations of a relatively high amplitude. The trunk muscles deliver maximum or close to maximum mechanical power output during this swimming mode.

A major question is how the movements of the body are produced by the trunk muscles. This problem has been tackled by various methods. Blight (1976, 1977) used electromyography to study the phases of activity of the trunk muscles in newt larvae and tench at various positions along the trunk (Fig. 13a). He concluded that only a small phase shift exists in the recorded activity from anterior to posterior. Thus, at one side along the trunk, considerable overlap occurs in the activity phase of the muscle fibres. With other words, these observations suggest the caudally running wave of lateral bending of the body to be produced by an almost alternating tension development in the axial muscles from side to side. These findings got further support by work of Hess and Videler (1984). They applied the inverse dynamics approach (Sect. 3.2) to fish swimming. They recorded the movements of saithe during continuous swimming, and calculated the forces on the body using a hydrodynamic theory outlined by Lighthill (1960). From these data, they calculated the net bending moment the fish should have generated along its trunk as a function of time. Figure 13b shows the amplitude of the bending moment along the trunk. The bending moment showed hardly any phaseshift along the trunk, in contrast to the curvature of the body (Fig. 13c). These calculations cannot tell by which structures (mainly muscle fibres and connective tissue) the bending moments are produced. For this purpose, a (validated) distribution model (Sect. 3.2) is required which is not available. Nevertheless, the muscle fibres produce probably force in phase with the calculated net bending moment. Hess and Videler's analysis shows also that, anteriorly, bending moment and curvature fluctuation result in a positive mean power output. Owing to the phaseshift in curvature, the mean power output is negative in the caudal peduncle.

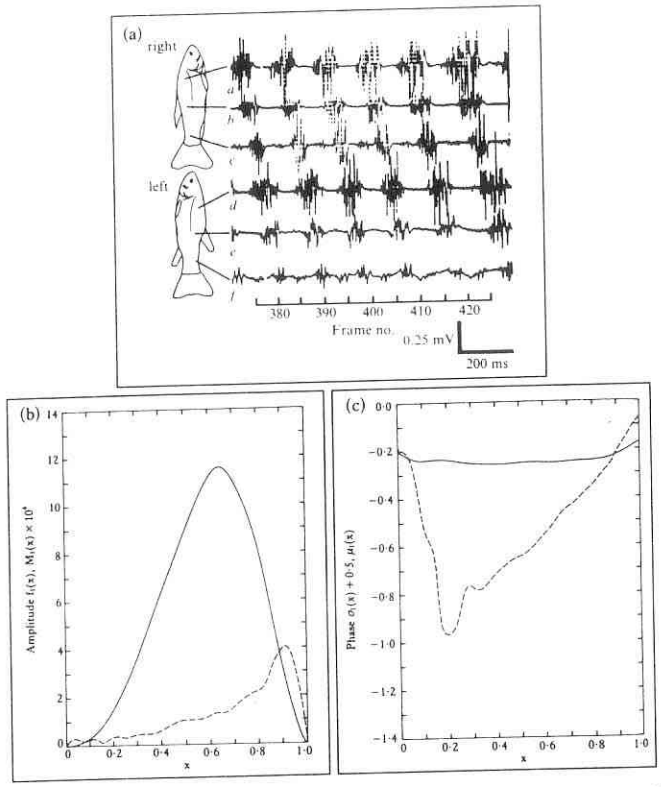

Fig. 13. **a** Electromyogram of tench (*Tinca tinca*) swimming muscles. (Blight 1976). During a short phase, muscle fibres are simultaneously active at one side of the body. **b** Calculated amplitude of bending moment (*continuous curve*) and curvature (*dashed*) in lateral bending along the body of a saithe. **c** Phase shift in bending moment (*continuous curve*) and curvature (*dashed*) along the body of a saithe. **b** and **c** reprinted Hess and Videler (1984)

The electromyographic analysis and the calculations of bending moments suggest that muscle fibres are active at different strain ranges along the body. Consequently, the muscle fibres along the body produce probably different amounts of power during the swimming cycle. Support for this suggestion came from an experimental and theoretical analysis of continuous and intermittent swimming carp by Van Leeuwen et al. (1990). They devised a method that can isolate the mechanical performance of single muscle fibres from the connective tissue. Their approach is summarized in Fig. 14. They aimed to calculate normalized forces, power and work during the swimming cycle. Only normalized quantities could be addressed since the number of involved muscle fibres could not be deduced. To this

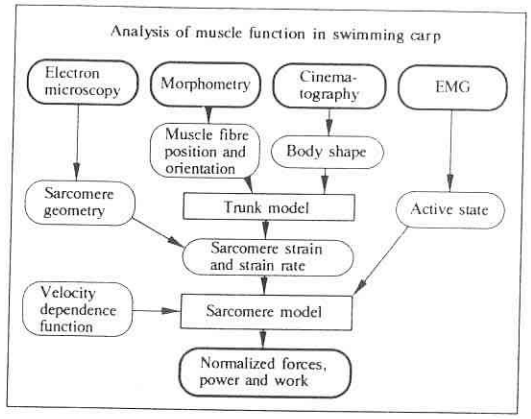

Fig. 14. Approach to study muscle fibre mechanical performance during swimming in carp as discussed in the text. (After Van Leeuwen et al. 1990)

aim a sarcomere model by Otten (1987a) was used, similar to that discussed in Sect. 2. This model requires four different types of input. First, the geometrical properties of the sarcomere (Sect. 2.1) should be known. These were obtained by electronmicroscopical observation of sarcomeres at four distributed positions along the trunk, as indicated in Fig. 15. From the measured parameters l_{myo}, l_{act}, l_{bz}, and l_z, the length dependence of force production was calculated.

Calculation of sarcomere force requires also knowledge about the velocity dependence function [Eq. (2)]. The part for positive interfilamentary sarcomere velocities was estimated from experimental data measured by Rome et al. (1988). For negative velocities (during stretching), an estimate was made on the basis of measurements by Aubert (1956). The third factor that Van Leeuwen et al. (1990) needed in their calculation was the active state. Therefore, the electrical activity of the red muscle fibres was monitored during continuous swimming at eight different positions along the trunk (Fig. 15). A differential technique was used so as to obtain records of the local activity. Measurements were made at one side of the body only, since the recruitment pattern can be assumed to be similar at both sides, but out of phase with each other. During intermittent swimming, both sides were monitored with four spots each (Fig. 15). In combination with experimental twitch data of muscle fibres of carp (time to peak tension is about 60 ms for slow fibres and 30 ms for fast fibres) by Granzier et al. (1983), the EMG records were used to estimate the active state.

Finally, data were required about the actual length fluctuations of the muscle fibres during swimming. Synchronously with the EMG records, high speed films were made of the fish swimming. A central axis of the fish was calculated from the digitized outlines of the fish. The strain and strain rate in the red (slow) muscle fibres was calculated from the local curvature of the central axis and the position and

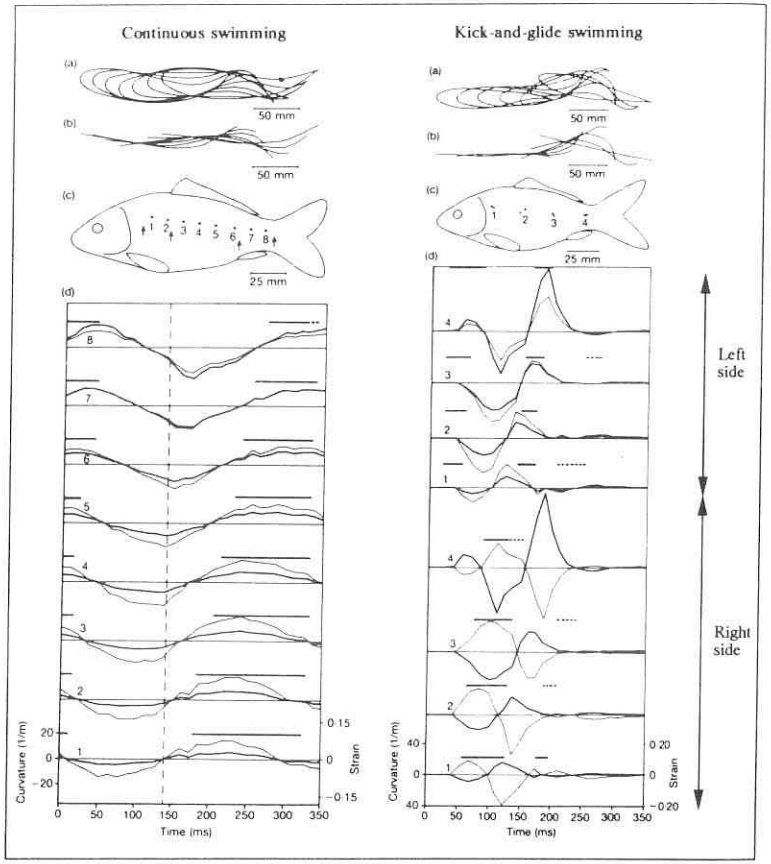

Fig. 15 a–d. *Left series of plots* Analysis of a close to continuous swimming cycle of a carp (SL = 156 mm). **a** Selection of measured outlines of the body. **b** Central axes, as calculated from the outlines. **c** Positions of electrode pairs at the *left side* along the trunk in the slow muscle fibres are numbered *1* to *8*. *Arrows* show sample positions of slow muscle fibres for ultrastructural observations. **d** Graphs of curvature of body axis (*heavy curves*, defined positive for bending to the right side), and the strain in the slow muscle fibres (*light curves*) at the electrode positions. *Numbers* correspond to those of **c**. The *horizontal bars* indicate the electrical activity of the slow muscle fibres. *Right series of plots* Analysis of a cycle of intermittent swimming of a carp (SL = 130 mm). Illustrations **a** to **d** are arranged similar to the left side. *Top four pairs* of graphs in **d** show curvature and strain on the left side of the fish (at positions corresponding to the dots in **c**). Other graphs show events from the right body side. Strain and curvature are out-of-phase at right side since curvature is defined positive for bending to the right side. *Broken horizontal bars* indicate weak electrical activity. (Van Leeuwen et al. 1990)

orientation of the muscle fibres with respect to the axis. The fibres lie as a thin (in cross-section triangular) strip directly underneath the skin. Details of the required assumptions and the calculations are discussed in Van Leeuwen et al. (1990). The calculations of the strain agree with sarcomere length measurements by Rome et al. (1988).

In continuous swimming (Fig. 15, left series of plots), the amplitude of curvature increased from anterior to posterior. However, the strain amplitude in the slow muscle fibres was constant along the trunk. Thus, in the posterior region, the higher amplitude of curvature was exactly compensated by the shorter distance between muscle fibres and body axis. During swimming without electrodes strain amplitudes were found of about ± 0.045. For swimming with electrodes this was ± 0.085, owing to an increased drag. In spite of the constant strain amplitude, the mechanical behaviour of the muscle fibres changed along the trunk since the fibres were activated at different intervals in their length cycle (Fig. 15d, left side). Anteriorly, the fibres started their electrical activity about 50 ms before peak strain, posteriorly this was about 90 ms. Anteriorly, the electrical activity lasted longest. The delay in activation over the trunk was shorter than the delay in the mechanical wave. The consequences for force and power output by the fibres will now be discussed.

Figure 16a shows the estimated active state along the trunk during the continuous swimming cycle at the 8 electrode positions, based on the data shown in Fig. 15 (simulation was started at the dashed vertical line of Fig. 15d). Activation was delayed and was shortened in a posterior direction. Active state decayed almost synchronously along the trunk. Force production (normalized to full isometric force, Fig. 16b) shows anteriorly an initial peak followed by a plateau in the shortening phase, and a final decay. Peak force (produced during forcible stretching) is below isometric force, owing to the low active state. In a posterior direction, peak force increases, whereas the plateau phase shortens. This is caused by an earlier activation in the lengthening phase, combined with a shortening in activation. Power production (normalized relative to maximum power, Fig. 16c) shows an initial negative peak over the complete trunk. This peak increases towards the tail, as expected from the length and force data. A power plateau, close to maximum power output, is present anteriorly. The plateau phase shortens towards the tail. In the caudal peduncle, only a small positive peak is left. The results may also be presented as work loops (force against length). Examples are shown for electrode position 2 (Fig. 16d, mainly positive work loop), position 6 (Fig. 16e, negative and positive part), and position 8 (Fig. 16f, negative work loop). Finally, Fig. 16g shows how the normalized work output per cycle changes along the trunk. In the anterior half of the trunk, work output is positive, it drops just in front of the anal region, whereas work output is negative at the most posterior two positions.

In intermittent swimming, the maximum curvature and muscle strain varied between successive tail strokes (Fig. 15, right series of plots). In the first tail stroke, the red fibres shortened actively at the left side of the fish (top half of Fig. 15d), while being under their resting length, except in the caudal peduncle where they were initially stretched when active. The minimum muscle strain decreased from anterior to posterior, and reached posteriorly values below -0.2. Muscle activity started almost simultaneously (within 5 ms) along the left body side. In the second stroke

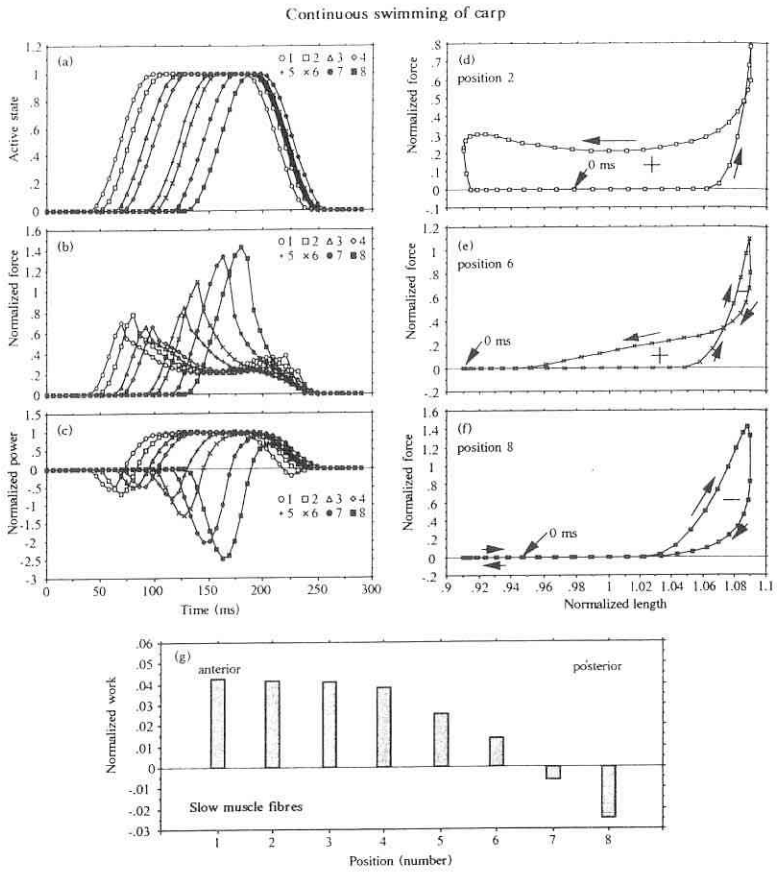

Fig. 16 a–g. Results from an analysis of red muscle fibre activity along the trunk during the continuous swimming cycle of Fig. 15 (*left series* of plots). The start of the analysis ($t = 0$ ms) is denoted by the vertical dashed line in Fig. 15d. *Curve numbers* correspond to the electrode position in Fig. 15. **a** Active state. **b** Force output, normalized relative to maximum isometric force at full activation. **c** Power output, normalized with respect to maximum power output. **d** to **f** Work loops at electrode positions *2, 6, 8* respectively. **g** Normalized work output ($W^*_{sarc} = W_{sarc}/(F_0 \cdot l_{0sarc})$) at the 8 electrode positions along the trunk. **a** to **f** after Van Leeuwen et al. (1990)

already, the start of muscle activity showed a wave character (right side of the fish, see bottom half of Fig. 15d, right side). Anteriorly, the muscle fibres mainly shortened while active, from above to below their optimum length. Only initially, the fibres were stretched during the activity period. Posteriorly, they were initially

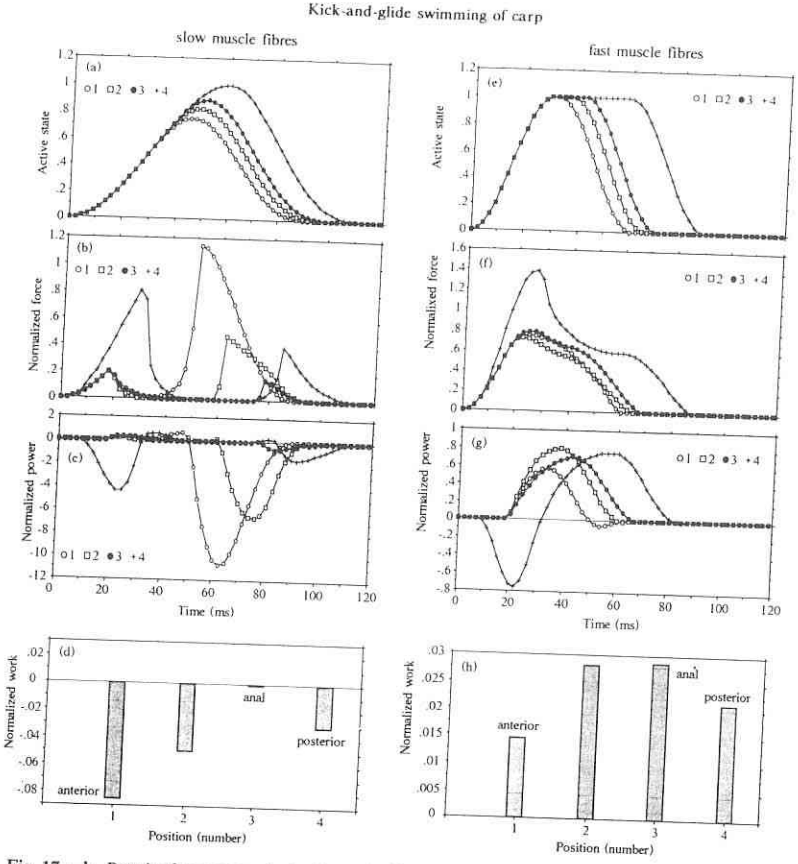

Fig. 17 a–h. Results from an analysis of muscle fibre activity along the trunk during the first tail strike of the intermittent swimming cycle of Fig. 15 (*right series* of plots). *Curve numbers* correspond to electrode positions shown in Fig. 15. **a** Active state of slow fibres. **b** Force output of slow fibres, normalized relative to maximum isometric force at full activation. **c** Power output of slow fibres, normalized with respect to maximum power output. **d** Normalized work output at the 4 electrode positions along the trunk. **e** to **h** are arranged similarly to **a** to **d**, but show predictions for white fibres. **a**, **b**, **c** based on data by Van Leeuwen et al. (1990). **e**, **f** and **g** after Van Leeuwen et al. (1990)

stretched and active above their resting length. Compared to the first stroke, this is a shift towards the pattern of continuous swimming.

The left side of Fig. 17 shows the results of a model analysis for the first tail strike after the glide phase in intermittent swimming. The swimming event shown in Fig. 15 served as a basis for this analysis. Van Leeuwen et al. (1990) reduced in their

calculations all the amplitudes in the strain curves by 50%. This was done because swimming with electrodes results in about twice the amplitudes as compared to swimming without electrodes. In contrast, model results will here be shown for the actual movement with electrode positions as shown in Fig. 15. The specific contraction speeds were such that hardly any force could be produced by the red fibres in their shortening phase. Thus, to generate the movement, the fish must have used its white and pink fibres. The stimuli along the trunk were so short that only in the caudal peduncle an active state of one was reached by the red fibres (Fig. 17a). The force curves for the examined electrode positions at the left side (Fig. 17b) show an initial peak, followed by a rapid decline owing to the high contraction velocities. In the caudal peduncle, the initial peak is highest, since the fibres were forcibly stretched (top half of Fig. 15d, right series of plots and Fig. 17a). The final peak in force production was caused by a final forcible stretching phase, with an increasing delay along the trunk. The normalized power curves (Fig. 17c) show that the red fibres produced mainly negative power, except in the anal region (position 3) where phases of positive and negative power almost compensated each other. The normalized work histogram (Fig. 17d) shows that energy was absorbed along the trunk during the first tail strike. In conclusion, the slow oxidative fibres could not have driven the observed movement.

How would the behaviour of the fast fibres have been during the "kick phase"? Figure 17e–h shows the results of a calculation, assuming that the activation periods of the fast fibres were equal to those obtained for the slow fibres. The required shortening speed of the fast fibres is less than that of the slow fibres, owing to their different orientation and position with respect to the axis (Alexander 1969). Based on Alexander's theory, Rome et al. (1988) estimated that white fibres only need to shorten at one fourth of the speed of the red fibres for a particular body curvature. Sarcomere length measurements of muscle fibres from specimens, fixed in a curved position, were consistent with this estimate. In one curved specimen, I measured a contraction ratio of slow fibres over fast fibres (number of samples was to small for statistical significance) of about 3 (electrode position 2 of continuous swimming) and about 4 for two other spots (electrode positions 4 and 6 of continuous swimming). Therefore, the strain fluctuations and contraction speeds were reduced in the calculations with a factor four compared to the red fibres (This is a correction of Van Leeuwen et al. 1990, who used a reduction factor of two). For the fast fibres, $\hat{v}_{max}$ was chosen to be 15 length/s (i.e. 2.73 times $\hat{v}_{max}$ of red fibres, based on measures by Rome et al. 1988). The velocity for maximum power output, V_p, was calculated to be 4.64 lengths/s (i.e. 3.05 times V_p used for the red fibres). The delay time, τ, for full force production was set to 30 ms, i.e. half the value the used for the red fibres (see also Granzier et al. 1983). The active state reaches now a value of one over the complete trunk (Fig. 17e). Compared to the red fibres, the force curves (Fig. 17f) are single peaked, owing to the shorter response time and increased $\hat{v}_{max}$. Peak normalized force in the caudal region is now larger than one during the initial lengthening phase, owing to the shorter response time. Figure 17g shows that anterior to the caudal peduncle, only positive power is produced, except anteriorly (position 1) in the final phase. Positive net normalized work is produced over the complete length of the trunk, with a maximum in the anal region (Fig. 17h).

In both swimming modes, contraction of anterior muscle fibres results in stretching of muscle fibres in or close to the caudal peduncle. Activity of muscle fibres in the caudal region costs energy. In fact, negative work could be done more efficiently with only collagen fibres, which can release stored strain energy. However, an advantage of muscle fibres is having the possibility of regulating the stiffness so as to obtain a better hydrodynamic efficiency. For fish, using different modes of swimming, this may result in a lower overall cost of locomotion, although the negative work of the posterior fibres (with little metabolic costs) has to be compensated by anterior muscle fibres doing positive work (at a much higher metabolic energy consumption). In conclusion, to obtain a high overall muscle efficiency, it may be required to work locally with a negative efficiency.

Can fish store useful strain energy in their muscles? Measurements by Altringham and Johnston (1990) show that the parallel elastic element is too compliant for this purpose. Elastic energy can also be stored in cross-bridges (Alexander and Bennet-Clark 1977). In continuous swimming, the fibres are activated during the final stage of the stretching phase. The stretch during activation is within 3%, so that cross-bridges can remain attached and store elastic energy. This mechanism will be most prominent in the caudal peduncle, where the highest levels of activation during stretching occur. The effect is, however, small compared to strain energy storage in a MTC.

4.2 Insect Asynchronous Flight Muscles

Asynchronous flight muscles, found in flies, beetles, bees, thrips, booklice and true bugs (Ellington 1985) are designed for a high frequency, low amplitude contraction regime. These muscles are particularly interesting, because some design principles come most brilliantly into focus owing to the extreme functional demands. In Sect. 2.6, two adaptations were already mentioned that optimize specific power output:

1. the complete overlap of actin and myosin as a structural optimization for specific myofibrillar power output during a short range contraction, and
2. the mechanically induced activation, reducing the required space for the SR (activation of synchronous muscles is also length-dependent, but neural input dominates, Sect. 2.2).

With the thorax and wings, the flight muscles form a resonance system. The resonance frequency of a damped spring-mass system can generally be increased if the effective mass and damping are decreased, and the spring stiffness is increased. This is accompanied by a very low amplitude of movement. The low effective mass is assured by the small size of the locomotor system, and the low density of air. The muscle fibres have also been found to have an exceptionally high passive stiffness (Machin and Pringle 1959; Fig. 18: lower curve). A delay between stretch activation and tension development ensures that active force is predominantly produced during shortening, so that positive work is done in each wing beat cycle (see work loop of Fig. 18). The origin of the delay is not fully understood, but Wray (1979) gives

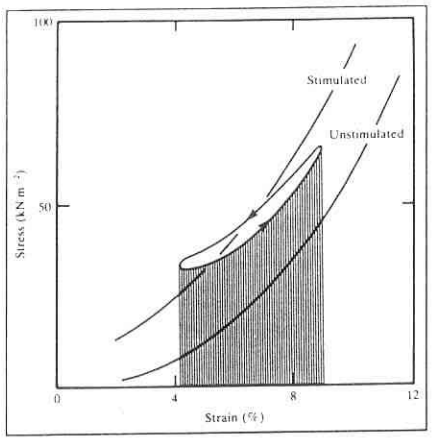

Fig. 18. Typical stress–strain curve for intact asynchronous flight muscle of *Oryctes rhinoceros* (stimulated and unstimulated) and oscillatory (work loop) conditions. *Shaded area* is proportional to absorbed work during stretch. *Loop area* represents net work done per cycle. (Ellington 1985, based on experiments by Machin and Pringle 1959)

an explanation based on filament geometry. Under natural conditions, stretching occurs dynamically by an inertial load. Machin and Pringle (1959) replaced the natural load of a flight muscle of a coconut beetle by an artificial load. Using an electronic circuit, various inertias, stiffnesses and damping influences were simulated. The self-oscillatory mechanism was disturbed if either the inertial load was very low or the damping very high. The high stiffness of the muscle, however, was kept intact. Most likely, the high stiffness originates from an exceptionally short and stiff c-filament, connecting the myosin filament to the Z-disc (White 1983). In this way, a passive spring is formed within the muscle, which can store a significant amount of elastic energy. During flight, the spring seems to be operated considerably above its slack length. This avoids the "toe" (left side in Fig. 18) of the nonlinear tension-length diagram, and assures relatively large fluctuations in the energy density function. The cross-bridges produce force in parallel to this spring and can also store elastic energy (Alexander and Bennet-Clark 1977). The strain fluctuations of the sarcomeres are so small ($\leqq 3\%$, that the myosin heads can, in principle, remain attached to the actin filaments throughout the wing beat cycle. Most likely, the cross-bridges produce force continuously, thereby elevating the effective stiffness of the system. Hence, favourable conditions for the absorption of kinetic energy of the wing mass and wing virtual mass at the end of the half stroke are present. The stored elastic energy is subsequently used to accelerate the wing in the next half stroke. As mentioned, the cross-bridges produce more force during the shortening phase than during lengthening, so that overall positive work is produced.

In buff-tailed bumble bee (*Bombus terrestris*), the musculo-skeletal system realizes the wing stroke amplitudes with very small sarcomere length changes (Dudley and Ellington 1990a, b). This insect uses the same wing beat frequency (about 160 Hz) and stroke amplitude over a wide range of flight speeds, from hovering to about 4.5 m/s. Flight speed is controlled by changing other parameters, such as body angle

and stroke plane angle. Therefore, the sarcomeres of the major flight muscles seem to operate similarly at various flight speeds. Dudley and Ellington (1990b) calculated that the required power output is also constant with flight speed. They estimated that all the kinetic energy of the wings could be stored in the flight muscles. These findings are consistent with the concept of a resonance system with a relatively fixed operating frequency.

4.3 Running and Jumping in Mammals: Muscles in Concert

This section deals with muscle function in terrestrial locomotion. An animal, walking or running at (a close to) constant speed, changes cyclically the potential and kinetic energy of its body. In walking, kinetic and potential energy fluctuations are more or less out of phase, since conversions between them are made by using the legs and body as an inverted pendulum (Chap. 4). This strategy saves metabolic energy. Elastic energy storage in tendons presumably plays a minor rôle as an energy saving mechanism, owing to the low forces in the muscles.

In running and hopping, the kinetic and potential energy fluctuate much more in phase, whereas the required muscle forces are much higher. Here, the potential for the muscles to use their build-in springs as strain energy stores are much higher (for reviews see Alexander 1984, 1988). In Sect. 2.7, it is shown that TTS stiffness should be "tuned" correctly to obtain a high efficiency. At slow running speeds, body segment accelerations and peak net joint moments are still relatively low. Elastic energy storage would be far from optimal if muscle activity were distributed rather evenly among synergistic muscles, since then the population of active fibres in each muscle would be in series with a relatively stiff TTS. If, however, some muscles or just one muscle from a synergistic group were active, then overall elastic energy storage would be more favourable. To continuously optimize elastic energy storage with increasing running speed, more muscles could sequentially be activated. At low speeds it would be most efficient to use muscles with mainly slow oxidative fibres. This principle of optimum efficiency may help to understand (1) the high number of muscles present in a leg, (2) distribution patterns of muscle fibre types over various muscles and (3) to predict activation patterns of synergistic muscle groups. It may also help to understand structural subdivisions within muscles. Similar to the swimming muscles of the carp, it is important to consider the overall efficiency of the muscular system.

The optimum efficiency hypothesis is supported by measurements of electrical activity, forces (using the tendon buckle method), and length changes of soleus (SOL) and medial gastrocnemius (MG) muscles in walking and trotting cat by Walmsley et al. (1978). They showed that the SOL is active at all speeds. Peak force production varies relatively little with locomotion speed. The MG, however, increases its peak force with running speed (Fig. 19d). The mechanism of strain energy storage during activated pre-stretch is used during running and jumping. Even during a fast trot, peak force in the MG (≈ 20 N) is relatively low compared to that in maximal jumping (Fig. 19c). Peak force is generated before peak MG length.

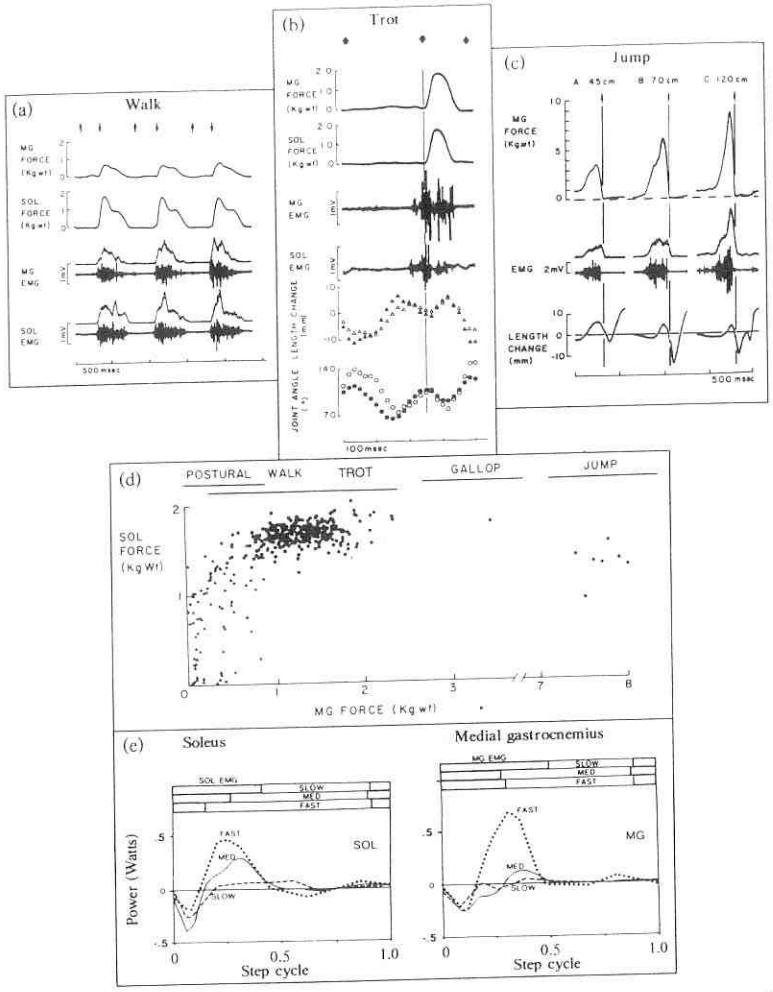

Fig. 19 a–e. Force and EMG (*upper EMG traces* in **a** and **c** are rectified and smoothed) records of cat soleus (*SOL*) and medial head of m. gastrocnemius (*MG*) during walking **(a)**, trotting **(b)**, and jumping **(c)**. Plot **d** shows peak force of MG against that of SOL during different activities. Read for *gallop* transition from trot to gallop. Force units are incorrect and should be multiplied by about 9.8 for conversion to N. (Walmsley et al. 1978). **e** Power output of SOL and MG during running at three different running speeds (Whiting et al. 1984)

During a transition from trotting to galloping, peak force was higher (about 35 N), which was accompanied with a shorter delay of peak length. During a high jump, peak force was highest (≈ 85 N), whereas peak length occurred simultaneously, or slightly later. These events are predicted by the MTC model of Sect. 2.7, as shown in the simulations of Fig. 11. With submaximal MG activation, the TTS is relatively stiff, compared to muscle fibre force. This would roughly resemble the simulation of Fig. 11 series 2. (In the simulations compared in Fig. 11, TTS stiffness is varied, in stead of activation levels. The relative effects, however, are similar). The relative TTS compliance is lowest in the jump, resembling roughly the situation of Fig. 11 series 3, with either coinciding force and length peaks of the MTC, or peak force slightly delayed to peak length. It is likely that the elastic properties of the TTS are best used during the jump, so as to obtain a (close to) optimum efficiency. Peak force of the SOL during the jump is lower than during running. This is caused by the high contraction velocities (Remember that the SOL contains mainly slow fibres). The cat would be able to jump higher if it had a faster SOL, but it would walk and trot less efficiently.

Further evidence for the present predictions comes from the work by Whiting et al. (1984), who studied the same muscles of the cat. They used also the tendon buckle technique to measure forces, but improved the measurements of length changes of both MTCs, so that estimates could be made of instantaneous power output (Fig. 19e). For the SOL, peak force and peak negative power decrease with an increasing running speed, whereas the positive power peak increases. This can be explained with the present MTC model. If only a fraction of the muscle fibres is activated, a relatively stiff TTS is experienced by them, resulting in a high muscle fibre stretching, more initial negative work of these muscle fibres, less elastic energy storage and presumably a lower MTC efficiency than with full activation. For the MG, it is mainly the positive power peak that increases with speed. More firm conclusions could be drawn if model simulations were made with the actual muscle parameters, in combination with various activation patterns.

In conclusion, activation patterns of muscles during locomotion are likely to be optimized so as to obtain optimum overall muscular efficiency during various levels of mechanical loading. Load sharing between synergistic muscles can so be predicted.

In terrestrial locomotion, most locomotor muscles work (in co-ordination with other muscles) in kinematic linkages such as legs. In principle, muscles might be constrained in their performance by the nature of the kinematic chain. The following discussion is mainly based on the work done on human jumping by Van Ingen Schenau and colleagues (reviewed by Van Ingen Schenau 1989), measurements of muscle moment arms by Spoor et al. (1990), and personal view points. Figure 20a illustrates some of the principle human leg muscles involved in a jump. The gluteus group (GLG) tends to extend the hip. The gluteus medius (GLME) and minimus (GLMI) are monoarticular. The gluteus maximus (GLMAX) inserts (with the biarticular m. tensor fasciae latae) for more than 50% on the tractus ilio-tibialis, a long tendinous part which passes the knee joint. Preliminary observations indicate that both muscles have an extending moment arm about the knee. (The treatment of the GLMAX as a strictly monoarticular muscle by Van Ingen Schenau c.s. and

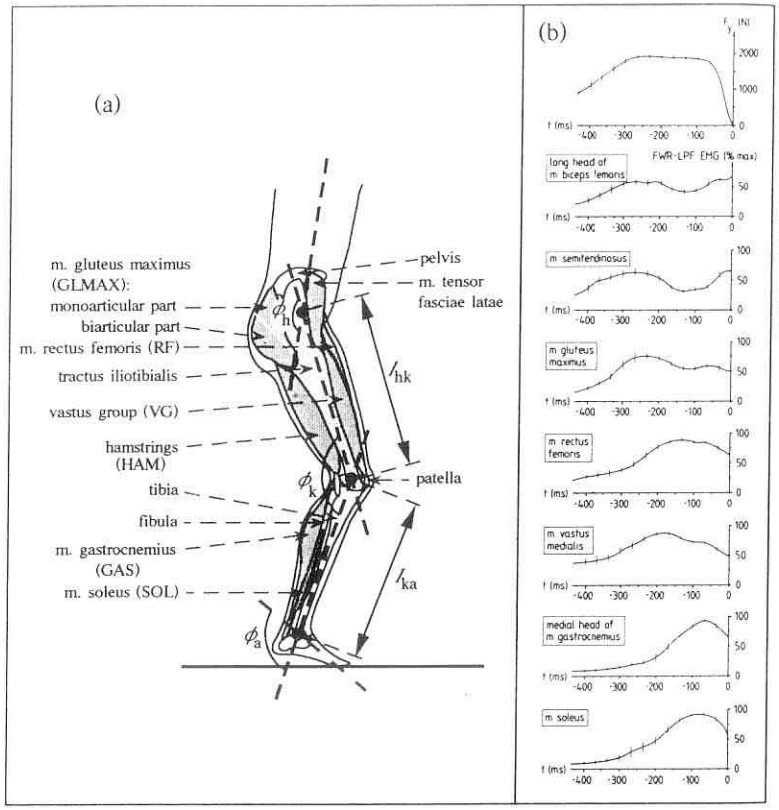

Fig. 20. **a** Diagram of important muscle groups involved in human jumping. Symbols ϕ_a, ϕ_k, and ϕ_h denote angles of ankle, knee and hip. *Dashed lines of heavy type* run through instantaneous centres of rotation of joints. **b** Ensemble averages ($n = 10$) of (1) vertical force on feet F_y and (2) rectified and low pass filtered electromyograms of some major leg muscles during the jump. Long head of m. biceps femoris and m. semitendinosus are parts of the hamstrings. *Vertical bars* show standard deviations. **b** Bobbert and Van Ingen Schenau (1988)

Pandy and Zajac (1990) is erroneous). The lesser part of the GLMAX is monoarticular. The vastus group (VG) tends to extend the knee. The SOL tends to extend the ankle (this usually is called plantar flexion; extension is used here since the rotation lengthens the leg). Several other muscles pass two joints. The hamstrings (HAM) tend to extend the hip and to bend the knee. The rectus femoris (RF) tends to flex the hip and extend the knee. The m. gastrocnemius (GAS) tends to flex the knee

and to extend the ankle. The phrase 'tend' is used because quite often joint rotations are opposite in direction to a particular muscle moment about the joint. For one-joint muscles, this always involves forcible stretching. For a biarticular muscle this may be the case.

Generally, the joints allow predominantly rotations to occur. Simple rules for the transformation from joint rotations to trunk rise can be derived if, for a moment, the joints are considered as planar hinges (Van Ingen Schenau 1989). First, we will consider a leg with only two segments. The hip height h in jumping can now be expressed as (using the law of cosines):

$$h = \sqrt{l_{hk}^2 + l_{ka}^2 - 2l_{hk} \cdot l_{ka} \cdot \cos \phi_k}. \tag{12}$$

where ϕ_k is knee angle, l_{hk} is thigh length (distance from hip joint to knee) and l_{ka} is crus length (distance from knee to ankle). The velocity of the hip is obtained by differentiation of formula (12):

$$v_h = \frac{dh}{dt} = [l_{hk} \cdot l_{ka} \cdot \sin \phi_k / \sqrt{l_{hk}^2 + l_{ka}^2 - 2l_{hk} \cdot l_{ka} \cdot \cos \phi_k}] \cdot \frac{d\phi_k}{dt}. \tag{13}$$

The expression between square brackets is the transfer function H from angular velocity to translational velocity v_h. Function H decreases to zero at $\phi_k = 180°$. Therefore, a jumper with a two-segment leg will be airborne before the knees are fully extended. For two reasons, this is unfavourable:

1. Towards full knee extension, a useful contribution to jumping could only be made with a sharply rising angular velocity. The muscles involved would not be able to keep up with this demand. Thus, the period when the most voluminous leg muscles would be able to contribute useful power to the jump is shortened.
2. At take-off, the thigh and crus have considerable angular velocities, representing an important source of kinetic energy which is not made available in a useful way to the jumping height. In fact, the segments would have to be decelerated to avoid knee damage. Thus, the efficiency would be low.

The restrictions to muscular performance by the above geometrical constraint are largely avoided by (1) the presence of a third segment (the foot), (2) the presence of biarticular muscles, and (3) appropriate changes in muscle moment arms with joint angulation.

Figure 21a shows the measured joint angles, joint angular velocities, net joint moments and net joint powers during a two-legged jump with a preparatory counter-movement (Bobbert and Van Ingen Schenau 1988). The subjects were encouraged to jump as high as possible. The jumping performance can be expressed as the sum of the potential and kinetic energy of the centre of mass of the body (CM) at the time of toe-off ($t_{to} = 0$ ms). The push-off phase, defined by an upward CM acceleration, started about 300 ms before t_{to} (-300 ms). During early push-off, hip extension is most prominent, knee extension starts at about $t = -200$ ms, whereas ankle extension starts at about -100 ms. The time sequence of the onset of joint extensions is associated with increasing activation levels of monoarticular muscles crossing the corresponding joints (Fig. 20b; remember that the mechanical response is delayed relative to the electrical activity, Sect. 3.1). All joint angular velocities diminish

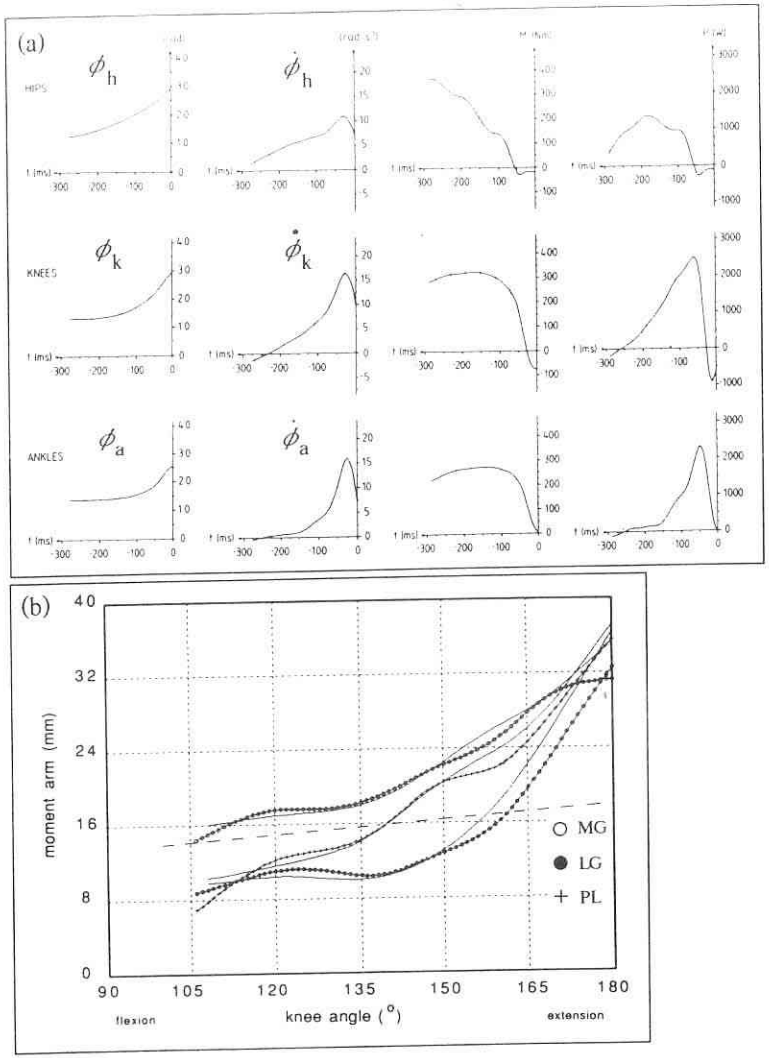

Fig. 21. **a** Mean time histories ($n = 10$) of hip, knee and ankle angles (for definition see Fig. 20), angular velocities, net moments of force (M) and net power output (P) at the joints. Time t is expressed relative to the instant of toe-off ($t = 0$ ms). Bobbert and Van Ingen Schenau (1988). **b** Measured moment arms of medial and lateral heads of gastrocnemius (*MG* and *LG*), and m. plantaris (*PL*) as a function of knee angle. *Unlabelled curves* show results of a repetition of the measurements. *Dashed line* is based on an (inaccurate) estimate by Grieve et al. (1978). (Spoor et al. 1990)

about 30 ms before take-off. In hip and knee, this is accompanied with negative moments, so that negative net power is produced in these joints. Peak net joint power is highest in the knee ($\approx$ 2500 W), it is only slightly lower in the ankle and considerably lower in the hip ($\approx$ 1500 W). This is in contrast to the volumes of the muscle crossing the joints (muscle fibre power output is proportional to muscle fibre mass). A consideration of muscle volume shows that the muscle fibres of the ankle extensors would not be able to generate the high peak net power output. The discrepancy is explained by (1) the actions of the biarticular muscles, evoking a mechanical coupling of joints and (2) rapid release of stored elastic energy in Achilles tendon and tendinous sheets of GAS and soleus.

The coupling action of a biarticular muscle is complicated owing to its complex dynamic properties (Sect. 2.7). The coupling is influenced for instance by the activation of the muscle fibres, instantaneous MTC length and velocity. Thus, coupling is by no means as strict as it would be with an inextensible string. The GLMAX and the HAM belong to the first muscles to become active during push-off (Fig. 20b). This helps to extend the hip. Initially, the knee angle varies very little during push-off (Fig. 21). Thus, upward acceleration of the CM is initiated by extension of the trunk. Knee extension is negligible in this phase, since a large external moment acts on the knee (the ground force has a much larger moment arm about the knee than about the hip in this phase). This effect is even enlarged by the active HAM (opposing knee extension), preventing an inertial force on the trunk which would hamper a high angular acceleration. The transfer from hip rotation to vertical translation of the trunk diminishes towards the vertical position. Knee extension comes into play when this transfer becomes less effective. Knee extension is supported by an increasing activation of the VG and RF and is favoured by a decreasing activity of the HAM. The contribution of the RF needs further consideration. The RF is a mechanical coupler of hip and knee. Hip extension during early push-off results in stretching of the RF, since the knee angle varies vary little up to $-$ 200 ms. During stretching, the activation level of the RF rises. Thus, strain energy will be stored in the RF. This energy originates (partly) from the GLG and HAM. Although the RF is continuously active, it is uncertain (although it seems likely) whether this strain energy is usefully released (catapult effect) in a subsequent shortening phase before t_{to}, since the net length change during the simultaneous extension of hip and knee is not known. A fine tuning of the activation is required to avoid energy losses owing to stretching of muscle fibres in the RF. Nevertheless, it can act as a force transmitter for the hip extensors, so that power generated by the hip extensors can show up in the net knee joint power. This helps to explain the simultaneous activation of both antagonistic groups. During knee extension, the transfer from rotation to translation becomes gradually less favourable [Eq. (13)]. An increasing activation of the GAS accomplishes that (1) kinetic energy due to the angular velocities of thigh and crus can be used to power ankle extension with still a favourable transfer from rotation to translation, and (2) muscle power from proximal muscles (mainly VG, but also GLG and others) can be used for ankle extension. This construction functions at the same time as an elegant shock absorber for the knee joint. Recent measurements of moment arms of the MG and LG by Spoor et al. (1990) support this view. Towards knee extension, the moment arms of

GAS about the knee almost double, owing to the build in shift of the axis of rotation of the knee joint. For the same reason, the moment arm of the quadriceps is likely to decrease towards full knee extension. This secures, with changing muscle activations, a rapid increase of the flexing moment about the knee. Again, part of the energy can be temporarily stored in the TTS of the triceps surae (Bobbert and Van Ingen Schenau 1988). This helps to explain also the overlap in activity between VG and GAS. A disadvantage of the usage of biarticular muscles as force transmitters are energy losses owing to viscous properties in the tendons and the muscle belly. It is of crucial importance that substantial stretching of muscle fibres is avoided (cf. Figs. 11 and 12). Finally, the foot has a low mass and therefore does not gain a high amount of kinetic energy.

In conclusion, it is likely that:

1. Biarticular muscles can help to improve the effective power output of monoarticular muscles, once muscle fibre stretching is avoided by a fine tuning of activation. Nevertheless, it remains to be proven that the energetic advantages dominate the energy losses in biarticular muscles.
2. Muscle moment arms about the knee vary so as to decelerate the knee angle towards full extension, and to make use of segmental kinetic energy to further heighten the CM through enhanced net ankle power output. Via the force transmitting limb bones, this power is transported to proximal segments. As explained by Pandy and Zajac (1991), the massive trunk segment gains most energy during the jumps, so that one can speak of an energy flow from the leg muscles in a proximal direction.
3. Kinetic and potential energy can be converted to strain energy in the various MTCs in a preceding counter-movement, and can therefore increase jumping performance.

A more complete understanding of the co-ordination of muscle activity during jumping can be obtained by the application of a direct dynamics analysis with appropriate MTC models for all leg muscles and including instantaneous variations of muscle moment arms. This would show the complete flow of mechanical power in the jumping apparatus. Search techniques could be employed to find optimum muscle activation patterns. A valuable step towards this goal was made by Pandy et al. (1990) and Pandy and Zajac (1991). They formulated a four-segment model, jointed together with frictionless revolutes, and driven by eight musculo–tendon actuators. The authors challenged the idea that jumping performance could be increased by the unique biarticular action of the GAS, by comparing simulated jumps (1) with all muscles, (2) with all biarticular muscles removed and (3) with all biarticular muscles removed, but with addition of a monoarticular GAS. Jumping performance was found highest in case (3) and lowest in case (2). For the following reasons, I doubt whether these findings allow the statement about the GAS:

a) The moment arms of the simulated muscles are very inaccurate, resulting for instance in a vanishing flexor knee moment of GAS towards knee extension (Pandy et al. 1990; Fig. 4b). This is a contrast to the increasing moment arms with knee extension as measured by Spoor et al. (1990). Since GAS is mainly active just before toe-off, I would indeed expect only a small calculated difference between a monoarticular and a biarticular GAS. In case (1), RF was calculated to have a significant negative work contribution. Therefore, the absence of RF in case (2) gives the highest jumping performance.
b) The linear stress–strain relationship of the tendons used by Pandy and Zajac (1991) might have led to a more than realistic muscle fibre stretching and, therefore, to an increased energy loss in biarticular muscles. Furthermore, contraction speed and activation dynamics were the same for all muscle–tendon actuators, whereas the well-known fast properties of the GAS may be essential to avoid an initial forcible muscle fibre stretching.

In conclusion, the direct dynamics approach is very promising, but it requires implementation of more accurate model description of muscles and joints before the issue of the rôle of biarticular muscles can be settled.

The above analysis considered jumping in a fairly large cursorial mammal. Owing to the required preceding counter-movement and the relatively compliant tendons, the jump is rather a time-consuming process. Small mammals (< 1 kg) apply several principles that allow a much quicker jump (i.e. with a higher, but shorter acceleration). First, they operate their legs in a much more flexed range of positions (Biewener 1989), with immediately a favourable transfer from rotation to translation [not requiring a substantial counter-movement, Eq. (13)]. Second, the tendons and aponeuroses of the muscles seem to be relatively stiff (Biewener et al. 1981), so that less time is consumed by an initial stretching of TTSs (similar to Fig. 9). Hence, muscle fibre power output appears with less delay as MTC power output, allowing a faster rise of CM kinetic and potential energy. Third, small mammals have a relatively higher number of fast muscle fibres (Goldspink 1977). Thus, small mammals, seem to be build for high accelerations (which might help to avoid predation by an escape response) as advocated by Biewener and Blickhan (1988) for the kangaroo rat. The disadvantage is a relatively high metabolic power consumption (Alexander and Ker 1990; Kram and Taylor 1990) since (1) elastic energy storage can only play a small rôle in locomotion (Biewener et al. 1981), (2) the noncursorial posture is inefficient and (3) fast muscle fibres are less economic than slow fibres (Goldspink 1977).

Even higher jumping accelerations can be obtained with yet another strategy, which uses the property that natural springs can release previously stored strain energy much quicker than a muscle can produce power. This strategy involves a relatively long process of energy storage in a natural spring (like an apodeme) by a muscle (as in Fig. 9 d–f). The jump is started with a click mechanism which triggers the quick release of the elastic energy. This strategy is especially important for small animals like insects (which have, owing to the short legs, very short acceleration times). A classical study of such a mechanism in the jumping locust is by Bennet-Clark (1975).

5 Conclusions and Perspectives

This chapter has shown how several well-known structural and functional properties of sarcomeres, muscles fibres and muscle–tendon complexes are effectively used in various locomotor systems. The diversity of structural design of sarcomeres was interpreted as a series of adaptations for optimum power output. In the last decade, much improvement has been made in the understanding of the timing of muscle activation of various locomotor systems. When actively stretched, muscle fibres produce much higher forces at very low metabolic cost than during shortening. This property allows the stiffness of the caudal peduncle of a swimming fish to be controlled at relatively low cost. It allows also an effective conversion of potential (associated with gravity) and kinetic energy of the body in elastic energy of stretched tendons and tendinous sheets, which can be released during subsequent shortening of the muscle–tendon complex (MTC). This requires an appropriate timing of activation as demonstrated with a dynamic MTC model, incorporating nonlinear properties of the contractile and tendinous system. Based on this model, an optimum efficiency principle was formulated for load sharing of synergistic muscles. The discussion of human jumping has indicated that biarticular muscles can distribute power from monoarticular muscles over various joints, and can help to convert segmental rotational energy to centre of mass energy.

The understanding of muscle function in locomotor systems is still largely based on EMG, force and strain measurements, muscle models and inverse dynamics analyses. Substantial further improvement may be obtained by a wider application of direct dynamics methods.

Acknowledgments. I thank Dr H.A. Akster, Professor R. McNeill Alexander, Drs. B. Gerritsen, Dr. M. Muller and Dr. C.W. Spoor for their helpful comments and interest. Professor M.G. Pandy and Professor F.E. Zajac are thanked for sending me papers that were still in press.

References

Aidley DJ (1975) Excitation contraction coupling and mechanical properties. In: Usherwood PNR (eds) Insect muscle. Academic Press, London, pp 337–356

Akster HA (1981) Ultrastructure of muscle fibres in the head and axial muscles of the perch (*Perca fluviatilis* L.). A quantitative study. Cell Tissue Res 219: 111–131

Alexander R McN (1969) The orientation of muscle fibres in the myomeres of fishes. J Mar Biol Ass 49: 263–289

Alexander R McN (1984) Elastic energy stores in running vertebrates. Am Zool 24: 85–94

Alexander R McN (1988) Elastic mechanisms in animal movement. Cambridge Univ Press, Cambridge

Alexander R McN (1989) Muscles for the job. New Sci 1660: 50–54

Alexander R McN, Bennet-Clark HC (1977) Storage of elastic strain energy in muscle and other tissues. Nature (Lond) 265: 114–117

Alexander R McN, Ker RF (1990) Running is priced by the step. Nature (Lond) 346: 220–221

Altringham JD, Johnston IA (1990) Modelling power output by a swimming fish. J Exp Biol 148: 395–402

An KN, Takahashi K, Harrigan TP, Chao EY (1984) Determination of muscle orientation and moment arms. J Biomech Eng 106: 280–282

Aubert X (1956) Le couplage énergetique de la contraction musculaire. Thesis, Arscia, Brussels

Barnes GRG, Pinder DN (1974) In vivo tension and bone strain measurement and correlation. J Biomech 7: 35–42

Barrett B (1962) The length and mode of termination of individual muscle fibres in the human sartorius and posterior femoral muscles. Acta Anat 48: 242–257

Bennet-Clark HC (1975) The energetics of the jump of the locust, *Schistocerca gregaria*. J Exp Biol 63: 53–83

Bennett MB, Ker RF, Dimery NJ, Alexander R McN (1986) Mechanical properties of various mammalian tendons. J Zool Lond A 209: 537–548

Benninghoff A, Rollhaüser H (1952) Zur inneren Mechanik des gefiederten Muskels. Pflügers Archiv 254: 527–548

Biewener AA (1989) Scaling body support in mammals: limb posture and muscle mechanics. Science 245: 45–48

Biewener AA, Blickhan R (1988) Kangaroo rat locomotion: design for elastic energy storage or acceleration? J Exp Biol 140: 243–255

Biewener AA, Alexander R McN, Heglund NC (1981) Elastic energy storage in the hopping of kangaroo rats (*Dipodomys spectabilis*). J Zool Lond 195: 369–383

Biewener AA, Blickhan R, Perry AK, Heglund NC, Taylor CR (1988) Muscle force during locomotion in kangaroo rats: force platform and tendon buckle measurements compared. J Exp Biol 137: 191–205

Blight AR (1976) Undulatory swimming with and without waves of contraction. Nature (Lond) 264: 352–354

Blight AR (1977) The muscular control of vertebrate swimming movements. Biol Rev 52: 181–218

Bobbert MF, Van Ingen Schenau GJ (1988) Coordination in vertical jumping. J Biomech 21: 249–262

Bone Q (1978) Locomotor muscle. In: Hoar WS, Randall DJ (eds) Fish physiology, vol VII. Academic Press, New York, pp 361–424

Brand PW, Cranor KC, Ellis JC (1975) Tendon and pulleys at the metacarpophalangeal joint of a finger. J Bone Jt Surg 57 (A): 779–784

Brown LM, Hill L (1982) Mercuric chloride in alcohol and chloroform used as a rapidly acting fixative for contracting muscle fibres. J Microsc 125: 319–336

Burke RE, Levine DN, Tsaeris P, Zajack FE (1973) Physiological types and histochemical profiles in motorunits of the cat gastrocnemius. J Physiol Lond 234: 723–748

Cavagna GA, Dusman B, Margaria R (1968) Positive work done by a previously stretched muscle. J Appl Physiol 24: 21–32

Close R (1964) Dynamic properties of fast and slow skeletal muscles of the rat during development. J Physiol 173: 74–95

Cutts A (1986) Sarcomere length changes in the wing muscles during the wing beat cycle of two bird species. J Zool Lond A 209: 183–185

Dimery NJ (1985) Muscle and sarcomere lengths in the hind limb of the rabbit (*Oryctolagus cuniculus*) during a galloping stride. J Zool Lond A 205: 373–383

Dudley R, Ellington CP (1990a) Mechanics of forward flight in bumblebees I. Kinematics and morphology. J Exp Biol 148: 19–52

Dudley R, Ellington CP (1990b) Mechanics of forward flight in bumblebees II. Quasi-steady lift and power requirements. J Exp Biol 148: 53–88

Dul J, Johnston GE, Shiavi R, Townsend MA (1984) Muscular synergism-II. A minimum-fatigue criterion for load sharing between synergistic muscles. J Biomech 17: 675–684

Ebashi S, Endo M (1968) Calcium ion and muscular contraction. Prog Biophys Mol Biol 18: 125–183

Edman KAP (1979) The velocity of unloaded shortening and its relation to sarcomere length and isometric force in vertebrate muscle fibres. J Physiol 291: 143–159

Edman KAP, Elzinga G, Noble MIM (1978) Enhancement of mechanical performance by stretch during tetanic contractions of vertebrate skeletal muscle fibres. J Physiol 281: 139–155

Ellington CP (1985) Power and efficiency of insect flight muscle. J Exp Biol 115: 293–304

Ettema GJC, Huijing PA (1989) Properties of the tendinous structures and series elastic component of EDL muscle–tendon complex of the rat. J Biomech 22: 1209–1215
Ettema GJC, Huijing PA, Van Ingen Schenau GJ, De Haan A (1990) Effects of prestretch at the onset of stimulation on mechanical work output of rat medial gastrocnemius muscle–tendon complex. J Exp Biol 152: 333–351
Fick AE, Weber E (1887) Anatomisch-mechanische Studie über die Schultermuskeln. Verh Phys Med Ges Würzb 11: 123–152
Flitney FW, Hirst DG (1978) Cross-bridge attachment and sarcomere "give" during stretch of active frog's muscle. J Physiol 276: 449–465
Goldspink G (1977) Muscle energetics and animal locomotion. In: Alexander R McN, Goldspink G (eds) Mechanics and energetics of animal locomotion Chap. 3, Chapman and Hall, London
Gordon AM, Huxley AF, Julian FJ (1966) The variation in isometric tension with sarcomere length in vertebrate muscle fibres. J Physiol 184: 170–192
Granzier HLM, Wiersma J, Akster HA, Osse JWM (1983) Contractile properties of a white- and red-fibre type of the m. hyohyoideus of the carp (*Cyprinus carpio* L.). J Comp Physiol 149: 441–449
Granzier HLM, Burns DH, Pollack GH (1989) Sarcomere length dependence of the force-velocity relation in single frog muscle fibers. Biophys J 55: 499–507
Grieve DW, Pheasant S, Cavanagh PR (1978) Prediction of gastrocnemius length from knee and ankle joint posture. In: Asmussen E, Jorgensen K (eds) Biomechanics-VI-A, International Series on Biomechanics, Vol. 2A, Univ Park Press, Baltimore, pp 405–412
Hatze H (1981) Myocybernetic control models of skeletal muscle. Characteristics and applications. Univ South Africa, Pretoria
Haug EJ (1989) Computer aided kinematics and dynamics of mechanical systems. Volume 1. basic methods. Allyn and Bacon, Boston
Heglund NC, Cavagna GA (1987) Mechanical work, oxygen consumption, and efficiency in isolated frog and rat muscle. Am J Physiol 253: C22–C29
Heilmann C, Pette D (1979) Molecular transformations in sarcoplasmic reticulum of fast-twitch muscle by electro-stimulation. Eur J Biochem 93: 437–446
Hess F, Videler JJ (1984) Fast continuous swimming of saithe (*Pollachius virens*): a dynamic analysis of bending moments and muscle power. J Exp Biol 109: 229–251
Hill AV (1938) The heat of shortening and the dynamic constants of muscle. Proc R Soc B 136: 399–420
Hof AL, Van den Berg JW (1981) EMG to force processing I: an electrical analogue of the Hill muscle model. J Biomech 14: 747–758
Huxley AF, Niedergerke R (1954) Structural changes in muscle during contraction. Interference microscopy of living muscle fibres. Nature (Lond) 173: 971–973
Huxley HE, Hanson J (1954) Changes in cross-striations of muscle during contraction and stretch and their structural interpretation. Nature (Lond) 173: 973–976
Huxley AF, Simmons RM (1971) Proposed mechanism of force generation in striated muscle. Nature (Lond) 233: 533–538
Josephson RK (1985) Mechanical power output from striated muscle during cyclic contraction. J Exp Biol 114: 493–512
Julian FJ, Rome LC, Stephenson DG, Striz S (1986) The influence of free calcium on the maximum speed of shortening in skinned frog muscle fibres. J Physiol 380: 257–273
Ker RF (1981) Dynamic tensile properties of the plantaris tendon of sheep (*Ovis aries*). J Exp Biol 93: 283–302
Kram R, Taylor CR (1990) Energetics of running: a new perspective. Nature (Lond) 346: 265–267
Light N, Champion AE, Voyle C, Bailey AJ (1985) The role of the epimysial, perimysial and endomysial collagen in determining texture in six bovine muscles. Meat Sci 13: 137–149
Lighthill MJ (1960) Note on the swimming of slender fish. J Fluid Mech 9: 305–317
Loeb GE, Pratt CA, Chanaud CM, Richmond FJR (1987) Distribution and innervation of short, interdigitated muscle fibres in parallel fibered muscles of the cat hindlimb. J. Morphol 191: 1–17
Machin KE, Pringle JWS (1959) The physiology of insect fibrillar flight muscle II. Mechanical properties of a beetle flight muscle. Proc R Soc B 151: 204–225
Machin KE, Pringle JWS (1960) The physiology of insect fibrillar muscle. III. The effect of sinusoidal changes of length on a beetle flight muscle. Proc R Soc B 152: 311–330

Morgan DL (1977) Separation of active and passive components short-range stiffness of muscle. Am J Physiol 232: C45–C49
Offer G (1987) Myosin filaments. In: Squire JM, Vibert PJ (eds) Fibrous protein structure. Academic Press, London
Otten E (1987a) Optimal design of vertebrate and insect sarcomeres. J Morphol 191: 49–62
Otten E (1987b) A myocybernetic model of the jaw system of the rat. J Neurosci Methods 21: 287–302
Otten E (1988) Concepts and models of functional architecture in skeletal muscle. In: Pandolf KB (ed) Exercise Sport Sci Rev, vol 16. MacMillan, New York, pp 89–139
Page SG, Huxley HE (1963) Filament lengths in striated muscle. J Cell Biol 19: 369–390
Pandy MG, Zajac FE (1991) Optimal muscular coordination strategies for jumping. J Biomech 24: 1–10
Pandy MG, Zajac FE, Sim E, Levine WS (1990) An optimal control model for maximum-height human jumping. J Biomech 23: 1185–1198
Pearson AM, Young RB (1989) Muscle and meat biochemistry. Food science and technology. A series of monographs. Academic Press, San Diego, pp 235–265
Podolsky RJ (1964) The maximum sarcomere length for contraction of isolated myofibrils. J Physiol 170: 110–123
Poliacu Prosé L (1985) De functionele stabiliteit van de kat. Een experimentele en biomechanische analyse van de bijdrage van ligamenten en spieren. Thesis, Free Univ Amsterdam and Free Univ Brussels (in Dutch)
Pringle JWS (1972) Arthropod muscle. In: Bourne GH (ed) The structure and function of muscle, vol 1, 2nd edn. Academic Press, New York, pp 491–541
Pringle JWS (1975) Insect fibrillar muscle and the problem of contractility. In: Bolis L, Maddrell HP, Schmidt-Nielsen K (eds) Comparative physiology, functional aspects of structural materials. North-Holland, Amsterdam, pp 139–152
Proske U, Morgan DL (1987) Tendon stiffness: methods of measurement and significance for the control of movement. A review. J Biomech 20: 75–82
Purslow PP (1989) Strain-induced reorientation of an intramuscular connective tissue network: implications for passive muscle elasticity. J Biomech 22: 21–31
Rack PMH, Westbury DR (1969) The effects of length and stimulus rate on tension in the isometric cat soleus muscle. J Physiol 204: 443–460
Rack PMH, Westbury DR (1984) Elastic properties of the cat soleus tendon and their functional importance. J Physiol 347: 479–495
Rapoport I (1972) Mechanical properties of the sarcolemma and myoplasm in frog muscle as a function of sarcomere length. J Gen Physiol 59: 559–585
Rome LC, Funke RP, Alexander R McN, Lutz G, Aldridge H, Scott F, Freadman M (1988) Why animals have different muscle fibre types. Nature (Lond) 335: 824–827
Salmons S (1969) Report on the 8th International Conference on Medical and Biological Engineering. Biomed Eng 4: 467–474
Selvik G (1990) Roentgen stereophotogrammetric analysis – a review article. Acta Radiol 31: 113–126
Sherif MA, Gregor RJ, Liu LM, Roy RR, Hager CL (1983) Correlation of myoelectric activity and muscle force during selected cat treadmill locomotion. J Biomech 16: 691–701
Spoor CW, Van Leeuwen JL, Meskers CGM, Titulaer AF, Huson A (1990) Estimation of instantaneous moment arms of lower-leg muscles. J Biomech 23: 1247–1259
Stenonis N (Stensen N) (1667) Elementorum Myologiæ Specimen, seu Musculi Descriptio Geometrica, vol 2. Stellae, Florence, pp 61–111
Stephenson DG, Williams DA (1982) Effects of sarcomere length on the force-pCa relation in fast and slow-twitch skinned muscle fibres from the rat. J Physiol 333: 637–653
Stevens ED (1988) Effect of pH and stimulus phase on work done by isolated frog sartorius muscle during cyclical contraction. J Muscle Res Cell Motil 9: 329–333
Stevenson RD, Josephson RK (1990) Effects of operating frequency and temperature on mechanical power output from moth flight muscle. J Exp Biol 149: 61–78
Street SF (1983) Lateral transmission of tension in frog myofibrils: a myofibrillar network and transverse cytoskeletal connections are possible transmitters. J Cell Physiol 114: 346–364
Taylor CR, Weibel ER (1981) Design of the mammalian respiratory system. I. Problem and strategy. Respir Physiol 44: 1–10

Usherwood PNR (1967) Insect neuromuscular mechanisms. Am Zool 7: 553–582
Van den Bogert AJ, Hartman W, Schamhardt HC, Sauren AAHJ (1989) In vivo relationship between force, EMG and length change in the deep digital flexor muscle of the horse. In: Biomechanics XI-A, Free Univ Press, Amsterdam, pp 68–74
Van Ingen Schenau GJ (1989) From rotation to translation: constraints on multiple joint movements and the unique action of biarticular muscles. Human Movement Sci 8: 301–337
Van Leeuwen JL (1991) Optimum power output and structural design of sarcomeres. J Theor Biol 149: 229–256
Van Leeuwen JL, Lankheet MJM, Akster HA, Osse JWM (1990) Function of red axial muscles of carp (*Cyprinus carpio* L.): Recruitment and normalized power output during swimming in different modes. J Zool Lond 220: 123–145
Van Lookeren Campagne AAH, Te Kronnie G, Huijing PA (1988) Muscle and fibre length force characteristics and filament length of rat semimembranosus and gastrocnemius muscle. In: Carraro U (ed) Sarcomeric and nonsarcomeric muscles: basic and applied research prospects for the 90's. Unipress Padova, Padova, pp 525–530
Vrbová G, Gordon T, Jones R (1978) Nerve-muscle interaction. Chapman and Hall, London
Wallinga-DeJonge W (1980) Force development in rat skeletal muscle: measurements and modeling. Thesis, Enschede
Walmsley B, Hodgson JA, Burke RE (1978) Forces produced by medial gastrocnemius and soleus muscles during locomotion in freely moving cats. J Neurophysiol 41: 1203–1216
Wang K (1985) Sarcomere-associated cytoskeletal lattices in striated muscle. In: Shay JW (ed) Cell and muscle motility, vol 6. Plenum. New York, pp 315–369
Weis-Fogh T, Alexander R McN (1977) The sustained power output from striated muscle. In: Pedley TJ (ed) Scale effects in animal locomotion. Academic Press, London
White DCS (1983) The elasticity of relaxed insect fibrillar flight muscles. J Physiol 343: 31–57
Whiting WC, Gregor RJ, Roy RR, Edgerton VR (1984) A technique for estimating mechanical work of individual muscles in the cat during treadmill locomotion. J Biomech 17: 685–694
Woledge RC, Curtin NA, Homsher E (1985) Energetics aspects of muscle contraction. Monographs of the Physiological Society 41. Academic Press, London
Woltring HJ (1986) A Fortran package for generalized, cross-validatory spline smoothing and differentiation. Adv Eng Softw 8: 104–113
Wray JS (1979) Filament geometry and the activation of insect flight muscles. Nature (Lond) 280: 325–326
Zajac FE (1989) Muscle and tendon: properties, models, scaling, and application to biomechanics and motor control. In: Bourne JRV (ed) CRC critical reviews in biomedical engineering, vol 17. CRC Press, Baco Raton, pp 359–411

Appendix A
Symbols and Abbreviations

Symbols

Symbols labelled with * represent normalized quantities. Symbols labelled with represent specific quantities. "At rest" denotes not activated and not under tension

A_{f0}	physiological cross-section of the muscle fibres of a MTC: $A_{f0} = V_m/l_{f0}$
A_{t0}	slack cross-section of tendon(s) and tendinous sheets of a MTC
c	constant in formula (16)
c_1, c_2	constants in formula (5)

c_3, c_4, c_5, c_6	constants in formula (9)
d	$[Ca^{2+}]_{0.5}$ at optimum sarcomere length [formula (16)]
$\hat{E}_{met}$	specific metabolic energy consumption of a muscle belly during a lengthening-shortening cycle of a MTC (in J per unit muscle volume)
F_0	maximum active force generated by a sarcomere, under isometric conditions and full activation
$F_a; F_{a0}$	active state, $F_{a0} \leqq F_a \leqq 1$; active state of a resting muscle fibre
F_{cb0}	average active force generated by the available cross-bridges in a sarcomere, under zero shortening speed and full activation
$F_{cu0}; F^*_{cu0}$	active force of a sarcomere, under conditions of zero shortening speed and full activation; $F^*_{cu0} = F_{cu0}/F_0$
$f_l; f_{lmax}$	filamentary overlap function; maximum filamentary overlap
F_{mb}	force exerted by a muscle belly (sum of the forces of parallel elastic element and muscle tissue)
F_{mtc}	force exerted by a MTC
F_{mus}	force exerted by the muscle fibres of a muscle belly (not including force of parallel elastic element).
F_{pas}	passive length-tension diagram of a MTC
$F_{pas1}; F^*_{pas1}$	passive force of a sarcomere at short lengths, resisting the cross-bridge forces and assumed to be independent of contraction velocity; $F^*_{pas1} = F_{pas1}/F_0$
$F_{pas2}; F^*_{pas2}$	passive force of a sarcomere above optimum length, acting in parallel to the cross-bridge forces; idem, but normalized
F_q	force of muscle fibre in relation to $[Ca^{2+}]$ under steady-state conditions
f_s	stimulus frequency
F_{sarc}	"dynamic" force generated by a sarcomere [formula (3)]
F_t	force exerted on a tendon
F_u	interfilamentary velocity dependence function
h	hip height
H	transfer function from angular velocity to translational velocity
k	constant in formula (2)
l_{act}	length of actin filament in two adjacent sarcomere halves, minus l_z
l_{bz}	length of bare zone (devoid of myosin heads) on myosin filament
l_c	length of connecting filament
l_{cmax}	sarcomere length with maximal effective cross-bridge density; $l_{cmax} = l_{myo} + l_z$
$l_f; l_{f0}; l^*_f$	muscle fibre length; idem but at rest; $l^*_f = l_f/l_{f0}$
l_{hk}	thigh length
l_{ka}	crus length
$l_{mb}; l_{mb0}; l^*_{mb}$	length of muscle belly; idem but at rest; $l^*_{mb} = l_{mb}/l_{mb0}$
l_{min}	minimum sarcomere length in active force-length diagram (Fig. 3a, b). Note that l_{min} is a function of u
$l_{mtc}; l_{mtc0}; l^*_{mtc}$	length of MTC; idem but at rest; $l^*_{mtc} = l_{mtc}/l_{mtc0}$
$l_{mtcopt}; l^*_{mtcopt}$	optimum length of MTC; $l^*_{mtcopt} = l_{mtcopt}/l_{mtc0}$

l_{myo}	length of myosin filament
$(l_{myo}/l_{act})_{pmax}$	filament ratio for maximum power output
l_{0sarc}	sarcomere optimum length: length at which the maximum active force can be generated under isometric conditions and full activation
$l_{sarc}; l^*_{sarc}$	length of sarcomere including the thickness of one Z-disc; $l^*_{sarc} = l_{sarc}/l_{0sarc}$
$l_t; l_{t0}; l^*_t$	length of tendon(s) of a MTC; idem but at rest; $l^*_t = l_t/l_{t0}$
$l_{ts}; l_{ts0}; l^*_{ts}$	tendinous sheet length of a MTC; idem but at rest; $l^*_{ts} = l_{ts}/l_{ts0}$
$l_{tts}; l_{tts0}; l^*_{tts}$	$l_{tts} = l_t + l_{ts}$; idem but at rest; $l^*_{tts} = l_{tts}/l_{tts0}$
l_z	thickness of the Z-disc of a sarcomere
n_{acb}	number of available cross-bridges in sarcomere subunit
$\hat{P}_{met}$	specific metabolic power consumption of a muscle fibre (in W per unit muscle volume)
$\hat{P}_{metmax}$	maximum value of $\hat{P}_{met}$
$\hat{P}_{mtc}$	specific power output by a MTC (in W per unit muscle volume)
$P_{mus}; \hat{P}_{mus}$	power output by the muscle tissue of a muscle belly; idem but specific (in W per unit muscle volume)
$P_{par}; \hat{P}_{par}$	power output by the parallel elastic element of a muscle belly; idem, but specific (in W per unit muscle volume)
P_{sarc}	sarcomere power output
$P_t, P_{ts}; \hat{P}_t, \hat{P}_{ts}$	power output of the tendon(s) and tendinous sheets of a MTC, respectively; idem, but specific (in W per unit muscle volume)
$\hat{P}_{tts}$	$\hat{P}_{tts} = \hat{P}_t + \hat{P}_{ts}$
$\hat{P}_\sigma; P^*_\sigma$	metabolic power consumption per unit volume of muscle needed to produce unit mechanical stress; idem but normalized
R	normalized stimulus of muscle fibre
r_m	muscle moment arm
s	tendon displacement
t	time
t_s	duration of stimulus
t_{to}	moment of toe-off in a jump
$u; u^*$	within one sarcomere, the velocity of the myosin filament relative to the actin filament; $u^* = u/u_{max}$
u_{max}	the maximum value of u
u_{ref}	interfilamentary velocity for reference (i.e. frog) sarcomere
u_{sarc}	absolute contraction velocity of sarcomere; $u_{sarc} = 2u$
v_h	translational velocity of the hip
$\hat{v}_{max}$	maximum specific shortening velocity of a muscle fibre in optimum fibre lengths/s
V_m	muscle volume
$W_{sarc}; W^*_{sarc}$	mechanical work output by sarcomere from $t = t_a$ to t_b; $W_{sarc} = \int_{l_{sarc}(t_a)}^{l_{sarc}(t_b)} F_{sarc} dl_{sarc}$; idem, but normalized: $W^*_{sarc} = W_{sarc}/(F_0 \cdot l_{0sarc})$

$\hat{W}_{mtc}$	specific work output by a MTC during a lengthening-shortening cycle (in J per unit muscle volume)
$\hat{W}_{mus}$	specific work output by the muscle tissue of a muscle belly during a lengthening-shortening cycle of a MTC (in J per unit muscle volume)
$\hat{W}_{par}$	specific work output by the parallel elastic element of a muscle belly during a lengthening-shortening cycle of a MTC (in J per unit muscle volume)
$\hat{W}_t, \hat{W}_{ts}$	specific work output of the tendon(s) and tendinous sheets of a MTC during a lengthening shortening cycle of a MTC, respectively (in J per unit muscle volume)
$\hat{W}_{tts}$	$\hat{W}_{tts} = \hat{W}_t + \hat{W}_{ts}$
$\hat{W}_+$	specific work output by a MTC during the shortening phase of a lengthening-shortening cycle (in J per unit muscle volume)
$\alpha; \alpha_0$	pennation angle of the muscle fibres in a muscle belly; idem but at rest
Δt	duration of a sarcomere contraction
ε	sarcomere strain [Eq. (16)]
ε_e	critical strain of tendon and tendinous sheets above which a linear stress-strain relationship is assumed
ε_f	muscle fibre strain
ε_t	strain of tendon(s) and tendinous sheets of a MTC
$\phi; \phi_a; \phi_h; \phi_k$	joint angle; ankle angle; hip angle; knee angle
λ	number of myosin heads per unit length on the myosin filament
σ_{miso}	maximum isometric stress of muscle fibres at optimum length
σ_t	mechanical stress of tendon(s) and tendinous sheets of a MTC
τ_{ca}	time constant in process of Ca^{2+} release from the SR (Appendix B)
τ_1, τ_2	time constants in formula (17) (Appendix B)

Abbreviations

CM	centre of mass
EDL	m. extensor digitorum longus
EMG	electromyography
LG	lateral head of m. gastrocnemius
GAS	m. gastrocnemius
GLG	gluteus group of muscles
GLMAX	m. gluteus maximus
GLME	m. gluteus medius
GLMI	m. gluteus minimus
HAM	hamstrings muscles
MG	medial head of m. gastrocnemius
MTC	muscle–tendon complex
PL	m. plantaris
RF	m. rectus femoris
SEC	series elastic component
SOL	m. soleus
SR	sarcoplasmic reticulum
TTS	tendon(s) and tendinous sheets of a MTC
VG	vastus group of muscles

Appendix B
Excitation–Contraction Coupling

The Ca^{2+} release from the SR can be described with a first order differential equation (Otten 1987b):

$$d[Ca^{2+}]/dt = \{[Ca^{2+}]_{max} \cdot R(t) - [Ca^{2+}]\}/\tau_{ca}, \quad (14)$$

where $[Ca^{2+}]$ is the instantaneous Ca^{2+} concentration in the sarcoplasm, $[Ca^{2+}]_{max}$ is the maximum concentration, τ_{ca} is the time constant of the process, and $R(t)$ is the normalized stimulus as a function of time ($0 \leqq R \leqq 1$). For fast muscle fibres, τ_{ca} is shorter than for slow muscle fibres. This corresponds to a greater SR-surface (e.g. Akster 1981) and faster ATPase in the SR-membrane (Heilmann and Pette 1979) of fast fibres, enabling a faster control of $[Ca^{2+}]$. Under steady state conditions, the relationship between normalized force of a muscle fibre and pCa ($= -\log_{10}[Ca^{2+}]$) is a sigmoid curve (Stephenson and Williams 1982; Julian et al. 1986), which can be described by (Otten 1987b):

$$F_q = [Ca^{2+}]^b / \{[Ca^{2+}]^b_{0.5} + [Ca^{2+}]^b\}, \quad (15)$$

where $[Ca^{2+}]_{0.5}$ is the Ca^{2+} concentration for a 50% activation. For rat muscle fibres, Stephenson and Williams (1982) showed $[Ca^{2+}]_{0.5}$ to vary with sarcomere length. Their experimental data can be described by:

$$[Ca^{2+}]_{0.5} = 10^{-(c \cdot \varepsilon + d)} M, \quad (16)$$

where ε is the sarcomere strain, d is $[Ca^{2+}]_{0.5}$ at optimum sarcomere length, and c is a constant which depends on the fibre type. For slow rat muscle fibres at 20 °C: $c = 0.65$. Fast fibres are less sensitive to sarcomere length changes. A good fit of the experimental data is produced with $c = 2.6$. Different values are needed with other temperatures.

F_q can be viewed as a "drive" for force development under dynamic conditions. Myofibrillar activation under these conditions is adequately described by inserting F_q into a second order linear differential equation, describing an overcritically damped system:

$$\tau_1 \cdot \tau_2 \cdot d^2F_a/dt^2 + (\tau_1 + \tau_2) \cdot dF_a/dt + F_a = F_q, \quad (17)$$

where F_a is the active state ($F_{a0} \leqq F_a \leqq 1$), and τ_1 and τ_2 are the time constants which depend on the muscle fibre type. This equation can describe the experimental observation that, after stimulation, the rise time of force production is shorter than the relaxation time. The above simple phenomenological description of the activation process is useful in the study of power and work output of muscle fibres during locomotor activities (Sect. 4.1). An exception has to be made for asynchronous flight muscles of insects which are relatively insensitive to the free $[Ca^{2+}]$ (e.g. Aidley 1975), and which rely for a great deal on mechanical activation (Sect. 4.2). More detailed discussions on the excitation–contraction coupling can be found in Ebashi and Endo (1968), Hatze (1981), and Wallinga-DeJonge (1980).

Chapter 8

Energetics of Locomotion

T.M. Casey

Contents

1 Introduction

The capacity for sustained activity varies widely in animals. The metabolic organization of endotherms, ectotherms, and insects varies dramatically. In ectothermic vertebrates the maximal aerobic energy expenditure is about ten times the resting metabolic rate and just about equivalent to the resting metabolic rate of endothermic vertebrates (Bennett and Ruben 1979). For endotherms the maximal

Department of Entomology, Cook College, Rutgers University, New Brunswick, New Jersey 08903, USA

Advances in Comparative and Environmental Physiology, Vol. 11